Petroleum Science 22 (2025) 277–295

Contents lists available at ScienceDirect

Petroleum Science

journal homepage: www.keaipublishing.com/en/journals/petroleum-science

Original Paper

Evaluation of micro-dispersion on oil recovery during low-salinity water-alternating-CO_2 processes in sandstone cores: An integrated experimental approach

Jia-Xin Wang [a, b, c], Leng Tian [b, d, **], Can Huang [e], Xiao-Jiao Deng [f], Daoyong Tony Yang [g, *], Rui-Heng Wang [h], Jia-Hao Lin [i], Jin-Yang Wei [h]

[a] CNOOC Research Institute Co., Ltd., Beijing, 100028, China
[b] College of Petroleum Engineering, China University of Petroleum (Beijing), Beijing, 102249, China
[c] State Key Laboratory of Offshore Oil Exploitation, Beijing, 100028, China
[d] Research Center for Natural Gas Geology and Engineering, China University of Petroleum (Beijing), Beijing, 102249, China
[e] Exploration and Development Research Institute, Jianghan Oilfield Branch Company, Sinopec, Wuhan, 430223, Hubei, China
[f] PetroChina Oil, Gas and New Energy Company, Beijing, 100007, China
[g] Energy Systems Engineering, Faculty of Engineering and Applied Science, University of Regina, Regina, Saskatchewan, S4S 0A2, Canada
[h] Exploration and Development Research Institute of PetroChina Changqing Oilfield Company, Xi'an, 710018, Shaanxi, China
[i] No. 3 Gas Production Plant of PetroChina Changqing Oilfield Company, Wushenqi, 017300, Inner Mongolia, China

ARTICLE INFO

Article history:
Received 8 June 2024
Received in revised form
10 September 2024
Accepted 10 September 2024
Available online 11 September 2024

Edited by Yan-Hua Sun

Keywords:
Low-salinity water-alternating-CO_2 process
Micro-dispersion
Wettability alteration
Clay minerals
Electrical double-layer
Multiple ion exchange

ABSTRACT

Low-salinity water (LSW) and CO_2 could be combined to perform better in a hydrocarbon reservoir due to their synergistic advantages for enhanced oil recovery (EOR); however, its microscopic recovery mechanisms have not been well understood due to the nature of these two fluids and their physical reactions in the presence of reservoir fluids and porous media. In this work, well-designed and integrated experiments have been performed for the first time to characterize the in-situ formation of micro-dispersions and identify their EOR roles during a LSW-alternating-CO_2 (CO_2-LSWAG) process under various conditions. Firstly, by measuring water concentration and performing the Fourier transform infrared spectroscopy (FT-IR) analysis, the in-situ formation of micro-dispersions induced by polar and acidic materials was identified. Then, displacement experiments combining with nuclear magnetic resonance (NMR) analysis were performed with two crude oil samples, during which wettability, interfacial tension (IFT), CO_2 dissolution, and CO_2 diffusion were quantified. During a CO_2-LSWAG process, the in-situ formed micro-dispersions dictate the oil recovery, while the presence of clay minerals, electrical double-layer (EDL) expansion and multiple ion exchange (MIE) are found to contribute less. Such formed micro-dispersions are induced by CO_2 via diffusion to mobilize the CO_2-diluted oil, alter the rock wettability towards more water-wet, and minimize the density contrast between crude oil and water.

1. Introduction

Compared to the traditional waterflooding, either LSW or CO_2 has been found to show its superior recovery performance in a hydrocarbon reservoir (Webb et al., 2004; Mahani et al., 2011; Rotondi et al., 2014; Seccombe et al., 2016; Chai et al., 2022). Physically, the former improves oil recovery by adjusting the ionic compositions of the injected brine to manipulate the fluid–fluid and rock–fluid interactions (McGuire et al., 2005; Lager et al., 2008), while the latter enhances oil recovery due to CO_2

* Corresponding author.
** Corresponding author. College of Petroleum Engineering, China University of Petroleum (Beijing), Beijing, 102249, China.
E-mail addresses: tianleng2009@126.com (L. Tian), tony.yang@uregina.ca (D.T. Yang).

https://doi.org/10.1016/j.petsci.2024.09.011

Nomenclature

CO_2-LSWAG	Low-salinity water-alternating-CO_2
EDL	Electrical double-layer
EOR	Enhanced oil recovery
ESEM	Environmental scanning electron microscopy
FT-IR	Fourier transform infrared spectroscopy
GFM	Gas flow meter
HSW	High-salinity water
HSWAG	High-salinity water-alternating-gas
HSWI	High-salinity water injection
IC	Ion chromatography
IFT	Interfacial tension
LSW	Low-salinity water
LSWAG	Low-salinity water-alternating-gas
LSWI	Low-salinity water injection
MIE	Multiple ion exchange
MMP	Minimum miscibility pressure
NMR	Nuclear magnetic resonance
OOIP	Original oil in place
PV	Pore volume
SARA	Saturates-aromatics-resin-asphaltene
SWAG	Simultaneous water-alternating-gas
TAN	Total acid number
TBN	Total base number
TDS	Total dissolved solids
WAG	Water-alternating-gas
XRD	X-ray diffraction

dissolution, oil swelling, light-component extraction, IFT reduction, and wettability alteration (Yang et al., 2005; Yang and Gu, 2005; Ramanathan et al., 2016; Al-Abri et al., 2019; Wang et al., 2020). Co-injecting LSW and CO_2 in an alternative manner, i.e., CO_2-LSWAG, may offer a higher ultimate oil recovery than each individual agent by taking their synergetic EOR advantages (Pourafshary and Moradpour, 2016). Due to the nature of these two fluids and their physical reactions in the presence of reservoir fluids and porous media, no in-depth investigation has been made to identify the parameters dominating oil recovery in a CO_2-LSWAG process at the microscopic level, though such information is fundamentally and technically critical for evaluating and optimizing its field-scale performance.

In the early 1990s, modifications to the injected brine composition were found to influence oil recovery (Jadhunandan, 1990; Jadhunandan and Morrow, 1991, 1995; Tang and Morrow, 1999). Through primarily modeling with the multiple ion exchange (MIE) hypothesis as proposed by Lager et al. (2007), clay minerals are found to impose a significant impact on oil recovery for sandstone formations; however, such a positive effect on oil recovery in carbonate reservoirs where clay minerals are absent has not been made available (Yousef et al., 2010; Ghasemian and Riahi, 2021). In practice, the most common recovery mechanism is assumed to be wettability alteration induced by an increase in the local pH (Zhang et al., 2006) and the EDL (Ligthelm et al., 2009). Contradictory, the pH in the effluent during a LSWI process was experimentally observed to increase but oil recovery remains unchanged (Cissokho et al., 2010; RezaeiDoust et al., 2010; Wideroee et al., 2010). According to the EDL model, a decrease in salinity of the injected brine has a substantial effect on surface forces at the interfaces of oil/brine and rock/brine, decreasing oil adhesion and increasing electrostatic repulsion on the rock surface (Jaafar et al., 2009; Alotaibi et al., 2011; Nasralla et al., 2014; Hilner et al., 2015; Mahani et al., 2015a, 2015b, 2017; Siretanu et al., 2015; Alotaibi and Yousef, 2016). With mineral adhesion experiments, a greater adhesion force between crude oil and a mineral surface was found at a lower salinity and a fixed pH (Buckley et al., 1989; Buckley and Morrow, 1990).

As for a LSWI process, the industry consensus seems to be an alteration in wettability toward a state that is more water-wet, enhancing the oil recovery in a hydrocarbon reservoir (Tang and Morrow, 1999; Nasralla et al., 2011; Skrettingland et al., 2011; Emadi and Sohrabi, 2013), though the source of such wettability alteration is still uncertain. Physically, wettability alteration resulting from the LSWI cannot be viewed as the microscopically dominant recovery mechanism until micro-dispersion was first visually observed via experiments with micromodels (Emadi and Sohrabi, 2013; Sandengen et al., 2016). Afterwards, at an oil/water interface, micro-dispersions are identified to be reverse micelle-structure clusters of water molecules encircled by polar species in crude oil (Mahzari and Sohrabi, 2014, 2018). Such a micro-dispersion differs significantly from the standard definition of (micro)emulsification: 1) The micro-dispersion at the oil-LSW interface is formed spontaneously and does not require shear force or synthetic surfactants; 2) The micro-emulsion is essentially a swelling micelle, whose particle size (10–100 nm) lies between the micelle (1–10 nm) and the emulsion (100–500 nm), while the micro-dispersion is a reverse micelle structure with a smaller aggregation number and size; and 3) The micro-emulsion acts as a micelle with hydrophilic groups forming the outer layer and hydrophobic groups forming the core, whereas the micro-dispersion (as the reverse micelle) does the opposite. Using micro-fluidic measurements, Mehraban et al. (2020) demonstrated that injecting LSW induces oil swelling and wettability alteration, the latter of which significantly increases the microscopic sweep efficiency. Moreover, micro-dispersion formation along with partitions of surface-active chemicals has been determined to be the main mechanism responsible for improving oil recovery at an oil/water interface during a LSWI process (Mehraban et al., 2021).

Even though CO_2 can be used to improve sweep efficiency, its inherent constraints are closely associated with the unfavourably high mobility ratio and adversely viscous fingering. As a result, CO_2 has been injected alternatively with high-salinity water (i.e., high-salinity water-alternating-gas (CO_2-HSWAG)) (Yang et al., 2015) and low-salinity water (i.e., CO_2-LSWAG) (Moradpour et al., 2021). Since its inception (Caudle and Dyes, 1958) up to the most recent works (e.g., Rogers and Grigg, 2000; Ghedan, 2009; Yang et al., 2015; Afzal et al., 2018; Bhadran et al., 2019; Belazreg and Mahmood, 2020), such a hybrid injection of CO_2 and water has proven to improve sweep efficiency and injectivity more than continuous CO_2 injection. Recently, HSWI has been coupled with CO_2 flooding to show their synergistic benefits with respect to EOR; however, significant concentrations of multivalent and monovalent ions in the injected brine restrict CO_2 from being dissolved in the brine, resulting in a decreased sweep efficiency due to CO_2 override with more free gas (Dang et al., 2014). Such challenges can be addressed by implementing CO_2-LSWAG since the solubility of CO_2 in brine is increased as the ion concentration is reduced (Kulkarni and Rao, 2005) and lowering free gas results in more favourable mobility ratio and better oil swelling, and thus a higher oil recovery factor (Jiang et al., 2010; Ramanathan et al., 2016; Wang et al., 2022a, 2022b). With its high solubility in LSW, not only will CO_2 have its high diffusion in water so that the mobility ratio and displacement front will be favourably controlled (Pourafshary and Moradpour, 2016), but also can extract the light-components from residual oil to the CO_2 phase for boosting oil production/recovery (Yang and Gu, 2005; Aleidan and Mamora, 2010; Zolfaghari et al., 2013; Kumar et al., 2016). By using brines with various salinities to evaluate contact angles in both carbonate and sandstone cores, Teklu et al. (2016) discovered that a lower brine salinity facilitates altering surface of a rock sample to be more water-wet. Al-Abri et al. (2019) investigated the effects of LSWAG combined with other fluids on oil recovery in sandstone cores, among which the CO_2-LSWAG is found to increase oil recovery up to 23%; however, no attempts have been made to characterize micro-dispersions for

the LSWI and CO_2-LSWAG processes.

In this work, well-designed experiments have been conducted and integrated to characterize micro-dispersions and identify their EOR roles during CO_2-LSWAG processes. Firstly, two types of crude oil with different propensities to form micro-dispersions were prepared, while the amount of micro-dispersion formed at the oil/water interface was then measured using the distillation method. FT-IR tests were carried out to characterize the interfacial properties of the in-situ formed micro-dispersions, and then zeta potential tests were conducted to measure surface charges of rock particles and crude oils as well as cation exchanges. In addition to measuring both IFT and contact angle, displacement experiments monitored with NMR analysis on sandstone cores rich in clay minerals were conducted to characterize micro-dispersions with respected to oil recovery. Finally, such experimental measurements are evaluated and analyzed.

2. Experimental

2.1. Materials

2.1.1. Fluids

As for Crude A employed in this work, its physicochemical properties including SARA, TAN, and TBN analysis are tabulated in Table 1. In order to avoid possible interactions with clay minerals, Crude A was directly extracted from a carbonate oil reservoir containing no clay minerals in the Tarim Basin, China, ensuring that the oil sample is not contaminated with clay minerals. While the TBN and TAN were determined with the potentiometric titration in accordance with the ASTM 2896 and ASTM D664 standards, respectively, the asphaltene content was tested using the IP-143 standard procedure. As for Crude A, its ratio of TBN to TAN is 7.66 (i.e., 4.90/0.66) so that mixed-wet to oil-wet conditions would be induced during the experiments since it is the prerequisite for altering wettability during a CO_2 injection process (Yang et al., 2008a, 2008b; Hadia et al., 2012). Prior to the experiments, Crude A is centrifuged to eliminate any potential emulsion and dissolved solids.

To minimize the effect of impurities in the formation water, synthetic brines with salinities of 100,000 and 1000 ppm, respectively, were prepared for use in the displacement experiments. Table 2 lists the concentration of each salt that was used to formulate the synthetic brines. The ratio of monovalent to divalent ions is maintained at 4:1. Before being utilized in the subsequent experiments, all brines underwent a vacuum to eliminate any dissolved air. Also, CO_2 with a purity of 99.998% was supplied by the Guangke Ltd., Xi'an, China.

2.1.2. Core samples

To achieve consistent and comparable results, sandstone core plugs were drilled from a preserved core acquired from an oil reservoir. In this case, the four core plugs used in the displacement experiments monitored with NMR analysis and contact angle tests were cut from a sandstone core sample containing clay minerals from the Ordos Basin, China. It should be possible to obtain visible observations about the prospective influence of clay minerals on the CO_2-LSWAG effectiveness with a sandstone core. To prevent any potential interactions between the coring fluids and the reservoir cores, no water-based fluid was employed throughout the coring process. All organic materials in the core samples were eluted with a 9:1 volumetric mixture of methanol and dichloromethane in order to achieve consistent and reproducible tests.

Table 2
The formulated brines with the dissolved ions.

Brine	Brine composition, ppm		TDS, ppm
	NaCl	$CaCl_2$	
High-salinity brine	80000	20000	100000
Low-salinity brine	800	200	1000

In the left side of Fig. 1, four core slices with a thickness of 3.0 mm will be cut out from Sample #1 and used to measure contact angles, and then the remaining core plug with a length of 120.0 mm will be utilized in displacement experiments monitored with NMR analysis. Through the XRD analysis and highly magnified ESEM imaging from thin sections, the mineralogical compositions of the rock were determined. As can be seen from Fig. 2, the images scanned from the four thin sections show that the rock samples have satisfactory homogeneity, allowing us to evaluate and compare the corresponding results obtained from contact angle tests and NMR monitored-displacement experiments in the presence and absence of micro-dispersions. With the analysis of XRD providing further information presented in Table 3 for the mineralogical characteristics of rock samples, kaolinite is found to make up the majority of the clay component of the rock.

2.2. Experimental setup and procedures

2.2.1. Micro-dispersion characterization

Quantifying the in-situ formed micro-dispersion and identifying its main responsible compounds in the crude oil can facilitate evaluating and selecting the CO_2-LSWAG process in a hydrocarbon reservoir. In general, it is challenging to separate the micro-dispersion from bulk oil in the laboratory since it is typically formed at the oil/brine interface (Arhuoma et al., 2009a, 2009b). In this research, an efficient and consistent procedure has been established to quantify the in-situ formed micro-dispersion and identify the primary chemicals that are responsible for such a formed micro-dispersion.

The procedure for eliminating the natural reverse micelles (i.e., micro-dispersions) from the oil is schematically depicted in Fig. 3. Oil molecules related to micro-dispersions resulting from natural surfactants were removed from the oil as far as possible in order to prevent reverse micelles from forming in the later experiments. A series of contact tests were performed using the crude oil and brines chosen and prepared for the purpose of attempting to determine what amount of micro-dispersions occur in the oil phase when it comes into touch with the low-salinity brine. First, Crude A was centrifuged before use in various experiments at the temperature of 60 °C to ensure that any possible emulsion and dissolved solids have been removed. Then, the low-salinity brine and Crude A were brought into contact in a customized-design chamber for a period of 3 days to confirm that the oil/brine interactions had

Table 1
Crude oil properties.

Crude oil	SARA analysis, wt%				TAN, mg KOH/g	TBN, mg KOH/g	Viscosity @ 60 °C, mPa·s	Density, g/cm^3
	Saturates	Aromatics	Resins	Asphaltene				
Crude A	56.05	22.29	12.74	8.92	0.66	4.90	30.28	0.786

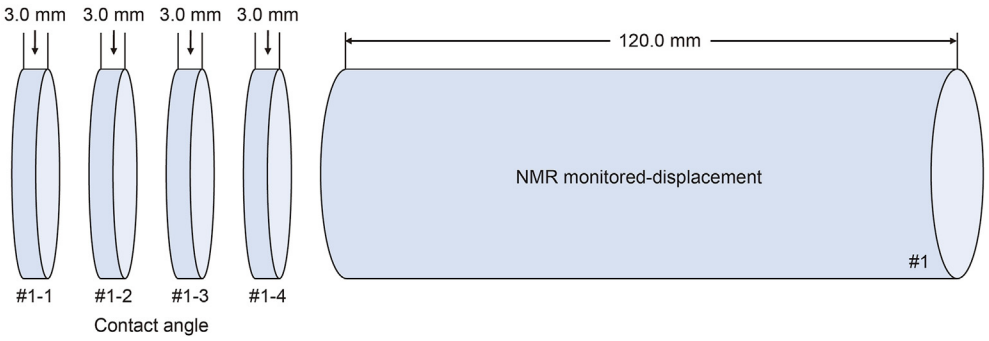

Fig. 1. Diagram illustration of the cutting locations of Sample #1.

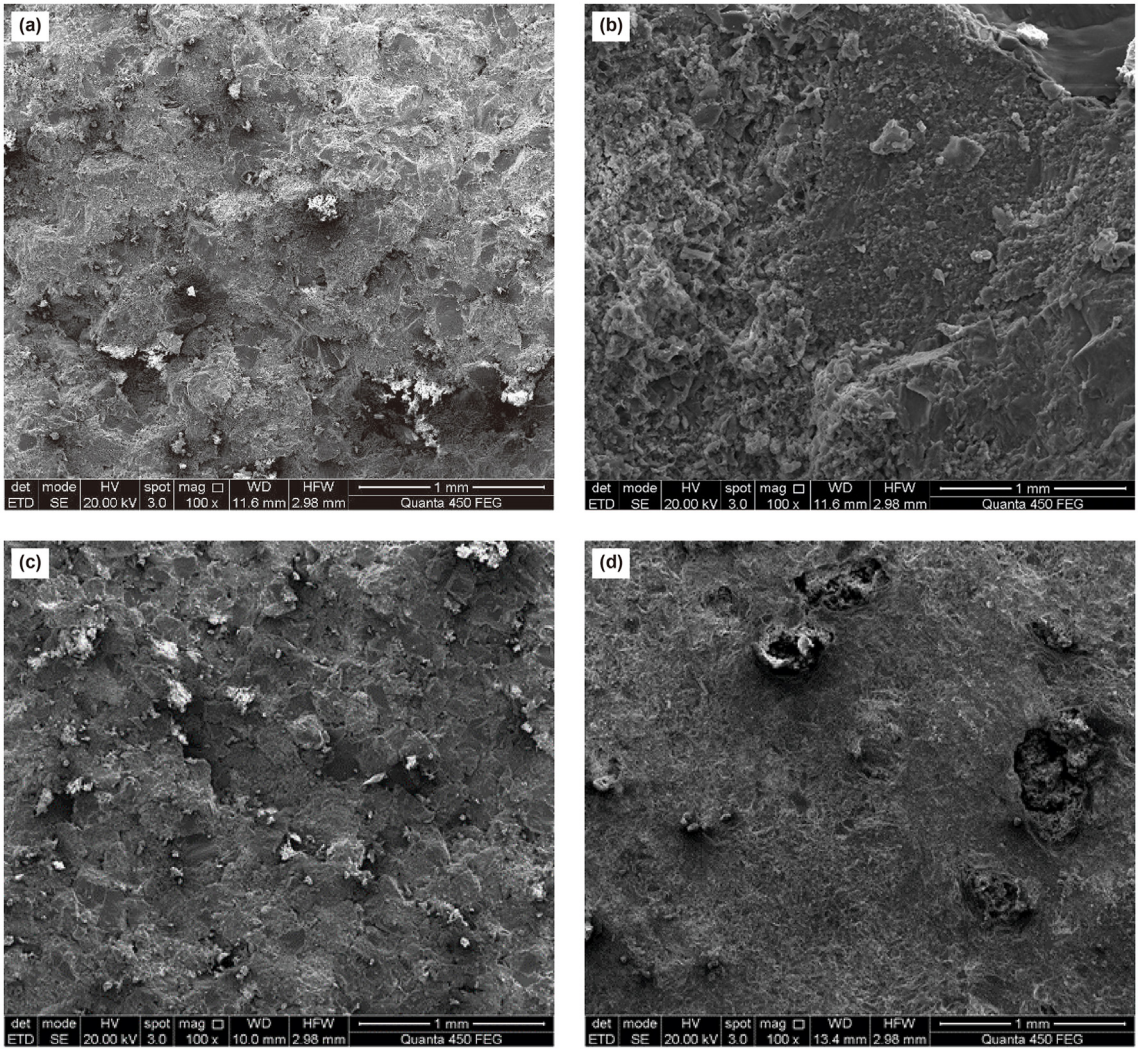

Fig. 2. ESEM images of the thin slices of #1-1 (**a**), #1-2 (**b**), #1-3 (**c**), and #1-4 (**d**) obtained from the cores.

Table 3
Mineral composition fractions determined via XRD analysis.

Mineral composition, wt%										Total, wt%
Quartz	K-feldspar	Illite	Kaolinite	Chlorite	Smectite	Muscovite	Calcite	Ankerite	Gypsum	
85.32	0.7	2.02	5.81	0.62	/	1.68	2.03	1.42	0.4	100

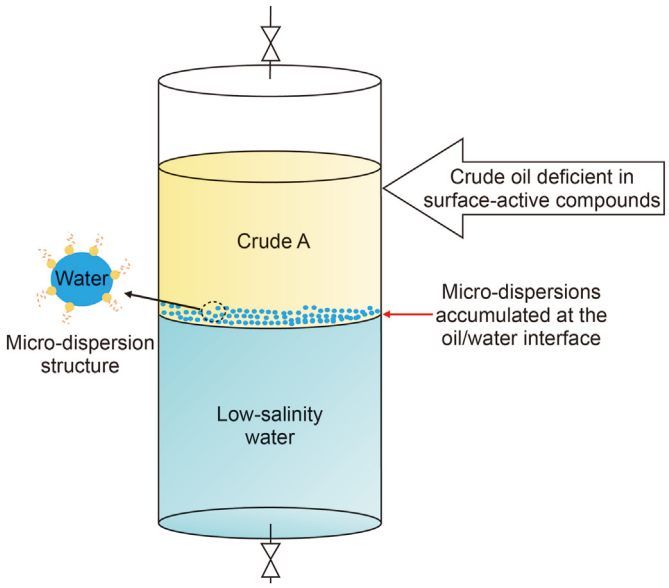

Fig. 3. A simplified diagram of the procedure for separating and extracting the reverse micelles (micro-dispersions) from Crude A.

achieved at an equilibrium state by following adsorption of surface-active materials from the bulk oil to the interface and the formation of micro-dispersion at the test temperature of 60 °C and pressure of 10 MPa. The oleic phase was cautiously removed without any physical agitation and the remaining oil was centrifuged to eliminate any gravitational micro-dispersions, resulting in a depletion of the surface-active chemicals associated with the low-salinity brine in the oleic phase at the top of the container. Subsequently, to determine the amount of micro-dispersion formed in-situ, the same procedure was followed for contact tests of crude oil with HSW, HSW-CO_2 mixture, and LSW-CO_2 mixture, respectively. The distillation method (i.e., ASTM D95) was employed for determining the amount of the water-in-oil (W/O) micro-dispersion (while experimental deviations were ensured to be less than 1% for the 3 measurements), during which CO_2 was supersaturated for the aforementioned mixtures.

The water concentration for the original Crude A was measured to be 0.011 vol%, which was utilized to normalize the amount of water in the crude oil after it has been made in contact with brines of varying ionic concentrations and CO_2. The micro-dispersion ratio is defined as the ratio of water concentration after the contact test to that before the contact test. Such a micro-dispersion ratio is employed to evaluate the potency of a crude oil to initiate micro-dispersion.

Subsequently, crude oil samples taken from different interfaces were analyzed using different analytical tools. Crude A (original) and Crude A-R (without micro-dispersion) were studied through FTIR spectroscopy, zeta potential, IFT, and contact angle measurements, respectively. The FTIR spectroscopy and zeta potential analyses provide valuable information about the identity of the surface-active materials responsible for micro-dispersion formation, while the IFT and contact angle measurements quantify the changes in IFT, wettability, and CO_2 dissolution conditioned to the in-situ formed micro-dispersion. Finally, the displacement experiments monitored with NMR analysis were conducted to examine the effect of micro-dispersions on oil recovery. In addition to the physical relationship, the diagram shown in Fig. 4 demonstrates the procedure that has been followed in this study for investigating the effect of micro-dispersion on oil recovery during CO_2-LSWAG processes.

2.2.2. Fourier transform infrared spectroscopy (FT-IR)

A TENSOR II IR spectrometer (Bruker, Germany) was utilized to perform FT-IR spectroscopy on the prepared crude oil samples. In total, 32 scans were employed for each crude oil sample that was deposited on the single-reflection glass window of the FT-IR spectrometer. For all of the oil samples, the IR spectrum was recorded in the 4000–400 cm^{-1} wavenumber region, provided that air was employed as the baseline to calibrate for the background spectrum. It is worthwhile noting that the glass window and potassium bromide slide were wiped with reagent grade toluene and methanol (Sigma-Aldrich Chemical Co., St. Louis, MO, USA) consecutively before and after each measurement, and then dried with pressurized nitrogen gas. Additionally, the equipped software OPUS and ORIGIN were employed for analyzing the scanned IR spectra of samples.

2.2.3. Zeta potential measurements

The zeta potential is a characteristic of colloidal solutions that specifies their surface charge. As the first (internal) layer of the EDL, the Stern layer is made up of a layer of ions charged oppositely to the surface and developed in an ionic solution at a charged surface, it is stationary in relation to the surface (Mehraban et al., 2020). An EDL will form once the particles enter the bulk solution and engage with other loosely coupled ions in the diffuse layer. The zeta potential values typically range from −100 to +100 mV (Hunter, 1981), while those less than −100 mV and more than +100 mV serve as a measure of colloidal stability of a solution (Shnoudeh et al., 2019). Temperature, ionic strength of the bulk liquid, and pH levels all have a profound effect on the zeta potential (Almeida da Costa et al., 2021).

Using a Zetasizer Nano-ZSP (ZEN5600, Malvern Instruments), the surface charges of crude samples were determined at ambient circumstances at a pH of 7. The electrophoretic mobility of oil droplets scattered inside a brine solution is determined via the Smoluchowski approximation of the Henry equation and then converted into zeta potential (Hunter, 1981). The ultrasonic probe (UP400St, SciMed Products Ltd) was applied to disperse 2.0 cm^3 of the centrifuged crude sample in 20.0 cm^3 of brine at a ratio of 1:10, while 5.0 cm^3 of the produced emulsion was combined with 50.0 cm^3 of parent brine, immediately following with ultrasound agitation and keeping on a magnetic stirrer for 1 h. Since CO_2 can significantly change the pH of the solution and impact the experimentally measured zeta potential (Almeida da Costa et al., 2021), the influence of CO_2 on crude oil is not considered due to its nonconductive nature.

To determine the zeta potential of rock particles, the ultrasonic probe was used to every scatter 5.0 g of rock particles with a size of 5.0 μm in 100.0 g of brine at a weight percentage of 5%. Such a prepared suspension was put on a magnetic stirrer immediately following with sonication to make sure it was keeping homogenized. The pH of the sample was adjusted using an acid/base titration with HCl (1 mol/L) and NaOH (0.1 mol/L). Depending on the level of purity and conductivity of the samples, the average of 5 tests with 13–100 runs per test is used to calculate each reported zeta potential value. Based on 5 measurements for each sample, there was a value deviation of about ±3 mV.

2.2.4. IFT measurements

The IFTs of CO_2/oil/brine systems were measured by digitizing and analyzing the measured pendant drop shape (see Fig. 5). As for the HSW-CO_2 and LSW-CO_2 mixtures, the fluids of interest in a high pressure cylinder are mixed and contained for 2 days to achieve the equilibrium state prior to measuring the IFT. Once a pendant oil

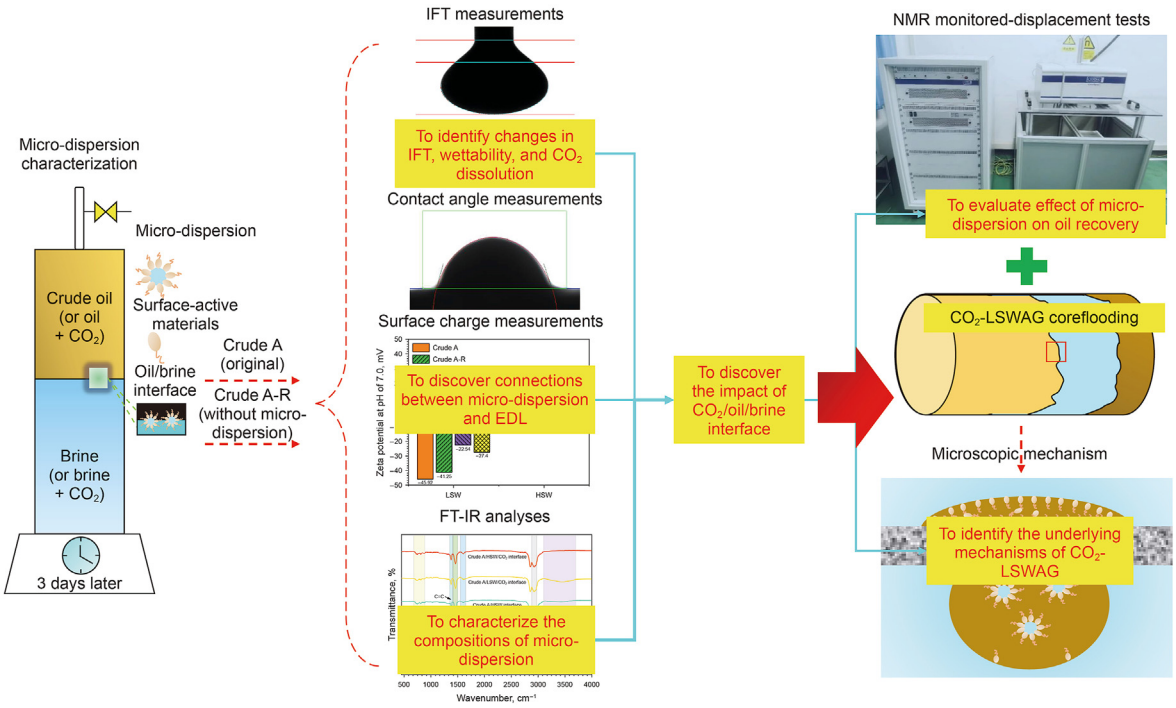

Fig. 4. Diagram of workflow for the experimental design.

drop has been introduced and well formed in the see-through cell, its image will be taken with the CCD camera and stored in a desktop computer, and then analyzed with the equipped ADVANCE software (Yang et al., 2005; Minch, 2018). By minimizing the difference of the digitized drop shape and the one estimated with the Laplace equation of capillarity, the IFT can then be determined at various conditions, depending on the fluid densities.

An oscillating tube densitometer (DMA 4200 M, $P_{max} = 50$ MPa, $T_{max} = 200$ °C; Anton Paar GmbH, Graz, Austria) equipped with a high-pressure injection system for gas-saturated solutions (HP ACC700, $P_{max} = 50$ MPa, $T_{max} = 200$ °C; Eurotechnica GmbH) was contracted to gauge the densities of crude oil, HSW, and CO_2-saturated LSW, respectively. The density for pure CO_2 at 60 °C was taken from Kunz et al. (2007). All IFT measurements were performed at 10 MPa and 60 °C, while experimental deviations were ensured to be less than 5% for the 5 measurements.

2.2.5. Contact angle measurements

The contact angle in the rock/oil/brine/CO_2 system was measured utilizing the captive drop method at 10 MPa and 60 °C (Fig. 5) (Yang et al., 2008a, 2008b). Four thin slices were obtained from a core plug (Sample #1) with a thickness of 3.0 mm and a diameter of 25.0 mm. The hydrocarbons from the core slices were eliminated utilizing a Soxhlet extractor, initially with toluene, followed by methanol, and then with toluene once more, till no oil traces were visible. After this, the slices were dried for 24 h at a

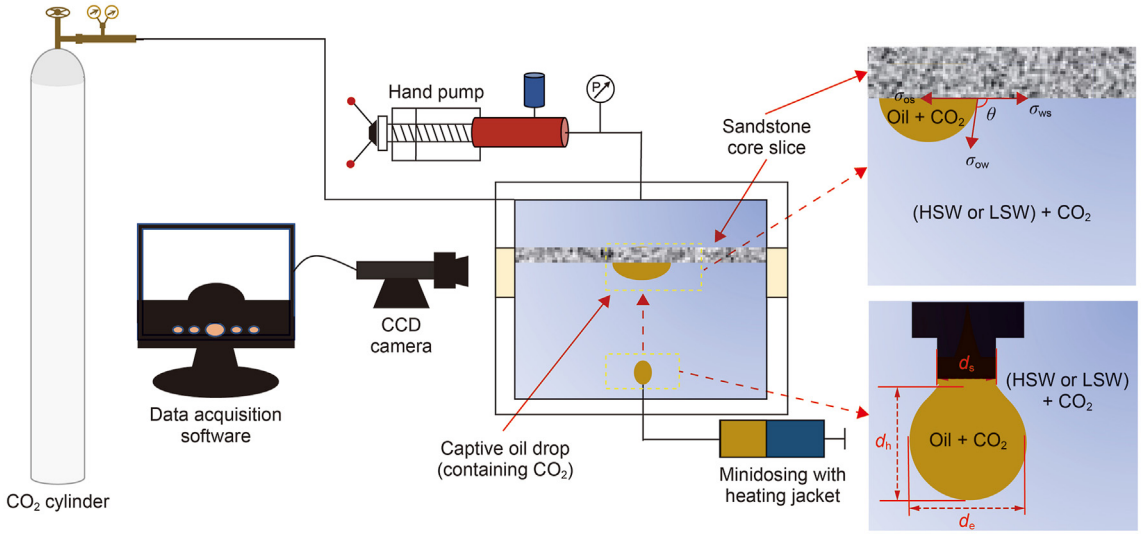

Fig. 5. Schematic of the experimental setup employed for determining the IFTs and contact angles of CO_2/brine/oil/rock systems.

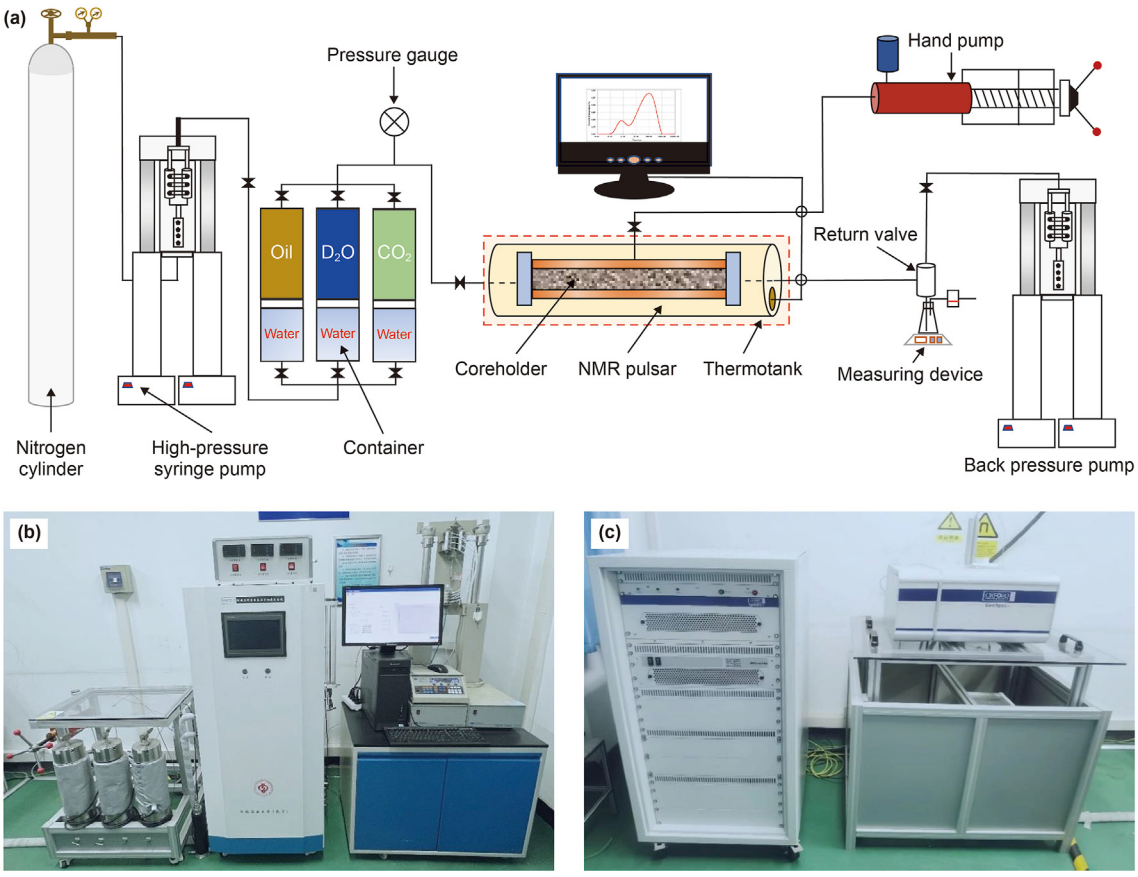

Fig. 6. (**a**) Schematic diagram of a displacement system integrated with an NMR apparatus; **(b)** An digital image of the injection subsystem; **(c)** An digital image of the NMR instrument.

Table 4
Physical parameters of core samples and initially conditions for the NMR monitored-displacement tests.

Crude oil type	Core plug	Length, cm	Diameter, cm	Porosity, %	Permeability (N_2), mD	S_{wi}, %	Flooding scenario	PV, cm^3
Crude A	#1	12.00	2.51	10.91	3.04	26.44	CO_2-HSWAG	6.42
	#2	12.00	2.51	10.35	2.64	17.62	CO_2-LSWAG	6.09
Crude A-R	#3	12.00	2.51	11.03	3.54	25.46	CO_2-HSWAG	6.49
	#4	12.00	2.51	10.89	2.64	15.38	CO_2-LSWAG	6.41

temperature of roughly 100 °C. Surfaces of core slices were smoothed (polished) with several grades (i.e., 30, 15, and 5 μm) of sandpaper in an increasing fineness, and a very-fine sandpaper of mesh is used to smooth the surface at the end. Once being polished, thin slices were immersed in a suction filter bottle for 10 h in order to enable its pores to be occupied with HSW, after which the saturated thin slices were aged with crude oil at 60 °C for 28 days. Note that the thin slices #1-1 and #1-2 were aged using Crude A (original), and thin slices #1-3 and #1-4 were aged using Crude A-R (without micro-dispersion).

With the aim of sweeping the additional oil layer off the rock surface and maintaining the oil droplet in contact with the surface of the aged core slice, crude oil was removed from the surface of each core slice using unbleached paper towels before contact angle measurements were performed. The wettability measurements are unaffected with the unbleached paper towel since it leaves no tiny particles on the surface of the core slice. Subsequently, a core slice was positioned over the prefabricated supporting frame inside the high-pressure vessel (OCA25L-PMC, DataPhysics Instruments GmbH, Germany) with transparent windows which had been washed with petroleum ether and vacuum dried. The synthetic brine was then added to the clean, dried pressure vessel and compressed to 10 MPa before being heated to 60 °C in a water bath. After 2–4 h of equilibration in the sounding fluids, a volume of 1–10 μL was dispensed from the bottom of the high-pressure cell via a stainless needle with an outer diameter of 0.632 mm to form a sessile drop beneath the thin slice. The thin slices #1-1 and #1-3 were submerged in HSW (100,000 ppm), while thin slices #1-2 and #1-4 were submerged in LSW (1000 ppm), respectively.

Supplemental contact angle measurements were carried out on crude-un-aged and crude-aged core slices, respectively, to examine the influence of CO_2 on wettability alteration. These measurements were then compared with those without CO_2. We injected super-saturated CO_2 into both oil and brine to imitate the reservoir condition of the CO_2-LSWAG process. More specifically, under experimental conditions of 10 MPa and 60 °C, thin slices #1-1 and #1-2 were kept for two days in a container inside a mixture of Crude A and CO_2 and thin slices #1-3 and #1-4 were kept for two

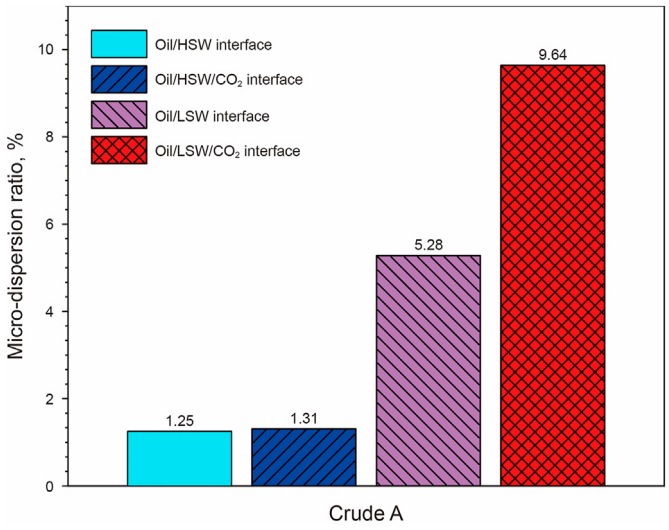

Fig. 7. Measured micro-dispersion ratio for Crude A at different interfaces.

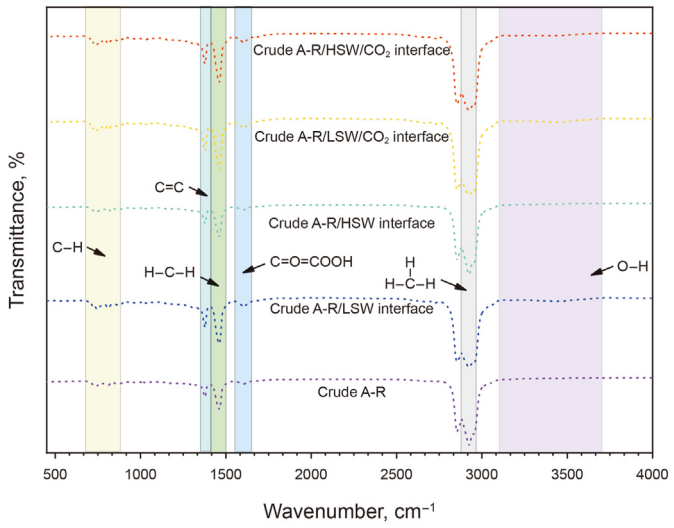

Fig. 9. FT-IR spectra of crude oil samples collected at the Crude A-R/LSW, Crude A-R/HSW, Crude A-R/LSW/CO_2, and Crude A-R/HSW/CO_2 interfaces.

days inside a mixture of Crude A-R and CO_2, respectively. Then, at 10 MPa and 60 °C, contact angles were measured between thin slices #1-1 and #1-3 and oil droplets by using the HSW-CO_2 mixture taken out of the cylinder as the surrounding fluid so as to simulate the reservoir condition of the CO_2-HSWAG process.

Similarly, contact angles were measured at 10 MPa and 60 °C between oil droplets and core slices #1-2 and #1-4 with the surrounding fluids being the LSW/CO_2 mixture obtained from the cylinder. This experimental situation was designed to replicate the reservoir status of the CO_2-LSWAG process. The pressure of 10 MPa was chosen in both measurement situations to simulate an immiscible CO_2 scenario as the minimum miscibility pressure (MMP) between Crude A and CO_2 is measured to be 21.36 MPa (Huang et al., 2024). One thing to note is that the crude oil used to form a sessile drop on an aged core slice for wettability measurement is the same as that used to age the rock slice. Furthermore, we measured the contact angle of un-aged core slices to evaluate and compare how reservoir wettability will be affected by secondary and tertiary recovery processes. It is worthwhile noting that this situation is the extremely possible scenario when the reservoir pore is "cleaned" after numerous pore volumes (PVs) of CO_2 have been injected.

The DSA-100 equipment (OCA25L-PMC, DataPhysics Instruments GmbH, Germany) was employed to determine the contact angles, and it has a high-resolution camera equipped with digital processing software. The reproducibility of the measurements was confirmed at least three times. Repeated experiments frequently indicate that the uncertainty of contact angle measurements is less than or equal to ±0.5°.

2.2.6. NMR monitored-displacement tests

Cores were saturated with high-salinity brines (100,000 ppm) prior to an NMR test. To make sure that all of the pores were in a vacuum state, the cores were first evacuated in a container. High-salinity brine was then pumped into the container under pressure. To ensure that the measured T_2 spectrum in a core plug after being saturated with water accurately reflects its distribution of pore sizes, the vessel is pressurized to 19 MPa using a piston pump. Finally, such a prepared core plug was positioned in a coreholder (KLQ-2, Yaping Ltd, Qingyang, China) and tested with an NMR pulsar (GeoSpec 253 Oxford Instruments, UK). The schematic representation of a merged displacement apparatus and NMR, consisting of a radio frequency emitter, a magnet, and a data gathering device, is shown in Fig. 6. The radio frequency with a 0.1 MHz control precision ranges from 1 to 30 MHz. Furthermore, the echo duration is 0.12 ms, the scanning number is 32, and the measurement period is 1.125 s. After the NMR analysis, the core plugs were dried at 100 °C for 12 h and cooled at room temperature for 12 h before being saturated again with vacuum and compressed to 19 MPa with high-salinity brine made with 99 wt% deuterium oxide at 100,000 ppm for 12 h. Using the displacement method, the deuterium oxide-filled cores were placed back in the coreholder and saturated with oil, while the outlet pressure and initial displacement pressure were kept as the atmospheric pressure and 2 MPa, respectively. The confining pressure was constantly maintained 2 MPa more than the displacement pressure. Notably, Samples #1 and #2 were saturated with Crude A, and Samples #3 and #4 were saturated with Crude A-R. The experiment requires a high-pressure syringe pump (Quizix5000, Broken Arrow, OK, USA) with a maximum displacement pressure of 60 MPa. The saturated oil process was continued until the outlet end stops producing

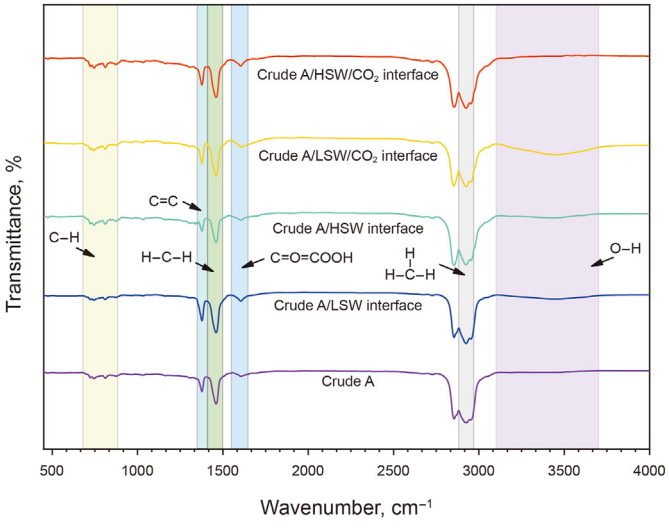

Fig. 8. FT-IR spectra of crude oil samples collected at the Crude A/LSW, Crude A/HSW, Crude A/LSW/CO_2, and Crude A/HSW/CO_2 interfaces.

Table 5
The peak areas for each functional group with the FT-IR analysis.

Interface sample	Peak area					
	C–H	C=C	H–C–H	C=O=COOH	H H–C–H	O–H
Crude A	5.95	3.16	16.09	2.25	15.45	2.96
Crude A/LSW	10.85	4.99	23.56	4.41	17.79	23.54
Crude A/HSW	9.88	3.72	18.52	2.98	15.58	14.98
Crude A/LSW/CO_2	11.75	5.14	24.15	5.04	18.09	58.62
Crude A/HSW/CO_2	6.82	4.62	22.03	3.58	17.99	7.89
Crude A-R	6.34	3.87	17.34	1.99	22.96	2.04
Crude A-R/LSW	8.56	4.75	25.46	2.05	15.23	8.38
Crude A-R/HSW	6.02	4.33	21.66	1.97	21.55	2.67
Crude A-R/LSW/CO_2	8.12	4.97	23.89	2.04	15.65	9.37
Crude A-R/HSW/CO_2	8.05	4.11	24.87	2.32	16.54	3.44

water for 12 consecutive hours and the displacement pressure was increased to 10 MPa and remains unchanged. After aging the oil-saturated core plugs for 28 days at experimental temperature and pressure, an NMR test was performed.

Table 4 lists the characteristics of the rocks and provides a brief summary of the NMR monitored-displacement tests. In this work, we injected HSW to simulate the reservoir situation following the secondary waterflooding and continually injected with LSW and CO_2 to assess the tertiary recovery performance. In each core plug, approximately 5 PVs of high-salinity brine were injected to displace the oil at a displacement pressure of 10 MPa. At this time, an NMR test was conducted to determine oil recovery during HSW flooding. Two core plugs (Samples #1 and #2) were used for Crude A, and two core plugs (Samples #3 and #4) were used for Crude A-R, respectively. Then, CO_2 injection was conducted at a WAG ratio of 5:3 and salinities of 100,000 ppm (Samples #1 and #3) and 1000 ppm (Samples #2 and #4), while the CO_2 slug size was 3 PVs. At the laboratory scale, the oil recovery is higher when the water-gas slug ratio is approximately 1:1. Because CO_2 flooding has a much higher oil recovery than water flooding, the slug size of injected water is appropriately expanded to highlight the influence of micro-dispersion on oil recovery during the LSWI stage. The NMR test was performed after each slug and the outlet pressure of the core was maintained at 8.0 MPa. To remove any capillary end-effects, two bumping floods were delivered at high injection rates of 0.5 and 1.0 mL/min at the conclusion of each displacement phase.

In order to achieve the immiscible flooding condition, the confining pressure was maintained at 12 MPa. The production fluids were gathered in a fraction collector during an HSWI or a LSWI process, and the brine and oil were collected in a graduated tube, centrifuged, and quantified. For CO_2 flooding, a separator was employed to gather the produced fluids and a gas flow meter (GFM) was employed to gauge the produced gas, while the produced brine and oil were collected with a graduated tube, centrifuged, and then measured. A thermotank (DHG-91140A, Hai'an, Nantong, China) with an accuracy of 0.2% was employed during the experiments in order to keep a constant temperature at 60 °C.

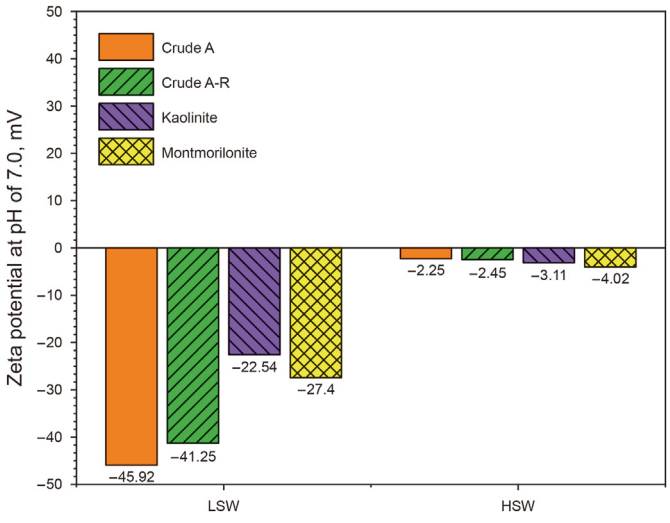

Fig. 10. Zeta potential of Crude A, Crude A-R, and other clay minerals in various brines at a pH of 7.0.

3. Results and discussion

3.1. Micro-dispersion characterization

As mentioned previously, the reverse micelles to form micro-dispersions were intentionally removed from the mixture of Crude A and LSW to make the prepared crude oil free of micro-dispersions (i.e., Crude A-R). To evaluate the formation of micro-dispersions, Crude A was contacted with HSW, HSW + CO_2, LSW, and LSW + CO_2, respectively, and the micro-dispersion ratio was calculated from the water content at the interface between the aforementioned fluids and crude oil samples.

According to Fig. 7, the micro-dispersion ratio is higher at the oil/LSW interface, illustrating that, when crude oil comes into contact with LSW as opposed to HSW, micro-dispersion tends to occur easier and its amount is monotonically increased as brine salinity is declined. After the supersaturated CO_2 was injected in a specially designed chamber containing both Crude A and brine at a pressure of 10 MPa and then kept for 3 days, the micro-dispersion ratio of the Crude A/LSW/CO_2 mixture was measured to be 9.64, which has been increased by 82.60% compared to that (5.28) of the Crude A/LSW mixture. Such an increase in the micro-dispersion ratio results from the unique physiochemical interactions between CO_2 and the Crude A/LSW mixture including CO_2 dissolution, oil swelling, light-component extraction, facilitating the formation of more microscopic water droplets encircled by polar oil components. This important observation provides a new perspective on the recovery mechanisms during a CO_2-LSWAG process, that is, CO_2 can promote the formation of micro-dispersions.

3.2. Compositional evaluation through FT-IR analysis

The FT-IR technique can be used to detect and differentiate bonds in a liquid, allowing us to compare and identify a given component and its concentration in crude oil. For example, FT-IR

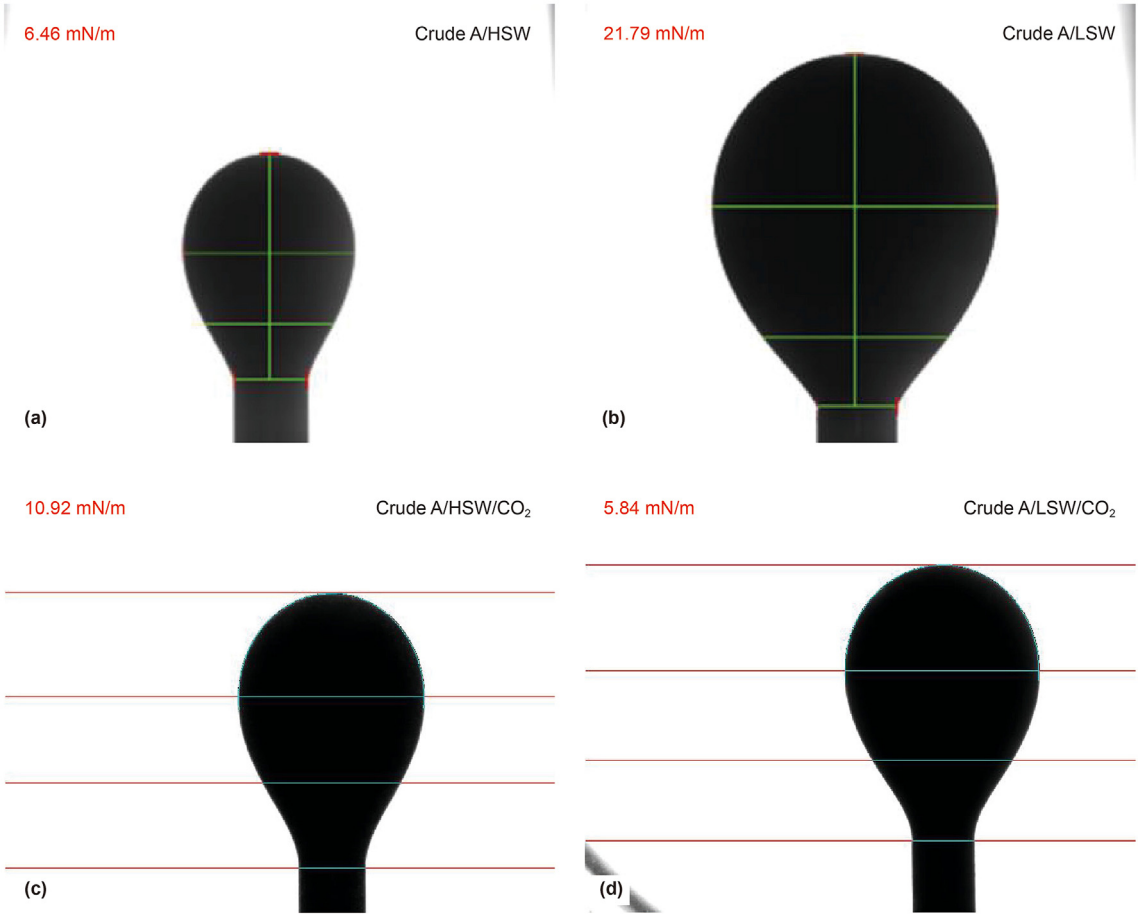

Fig. 11. Measured IFT for different systems at 60 °C and 10 MPa. **(a)** Crude A/HSW; **(b)** Crude A/LSW; **(c)** Crude A/HSW/CO_2; **(d)** Crude A/LSW/CO_2.

analysis has been utilized to evaluate rock wettability in crude oil/aqueous systems together with micro-dispersion characteristics (McDonald et al., 1986). As can be seen in Figs. 8 and 9, FT-IR analysis has been performed for crude oil samples being contacted with LSW, HSW, HSW + CO_2, and LSW + CO_2, respectively. It shall be noted that the *y*-axis represents transmittance which has a reverse connection to adsorption. Physically, a transmittance of 100% means that no IR radiation is absorbed by the sample. In this case, a lower transmittance at a particular wavenumber means a stronger adsorption of a specific chemical bond, while a difference in attenuation results from a change in the compositions of crude oil (Akhlaq, 1999).

As shown in Figs. 8 and 9, the FT-IR spectra show that the transmittances for all the aforementioned fluids and their mixtures have a similar pattern as a function of wavenumber with various areas covered under each peak. The number of bonds is found to increase with an increase in the area covered under the transmittance peak. Due to the transmittance of numerous bonds in crude oil, the measured FT-IR spectra may have their peaks superimposed at certain points, the quipped software is used to distinguish the boundary and position of the peaks as tabulated in Table 5.

There exist several distinctive bonds that show a favourable tendency to induce the in-situ formation of micro-dispersion. There are two other types of vibration bonds with lower intensities at 900–650 cm^{-1} and 1411–1358 cm^{-1}, which belong to the out-of-plane bending vibrations of the C–H and C=C bonds of aromatic rings, respectively. Also, there are vibration bonds at 1501–1412 cm^{-1} that correspond to the sp^2 carbons in a methylene group. The existence of the C=O bonds is indicated by vibrations with a wavenumber between 1550 and 1650 cm^{-1}. The C=O bonds probably represent carboxylic acids in crude oil, which are originated from the functional group COOH. The symmetric stretching vibrations of the sp^3 carbons in a methyl group are typically observed in one sharp bond in hydrocarbons at 2970–2830 cm^{-1} (Emadi and Sohrabi, 2013). Furthermore, the most essential vibratory bond for polar O–H bonds of either acidic materials or water molecules (i.e., containing the COOH functional group) is the broad peak at 3800–3100 cm^{-1}, which may be related to micro-dispersions at the oil/brine/CO_2 interface. All of those bonds might have polar properties (Qi et al., 2013) and interestingly, these bonds may be actively involved in wettability alteration induced by CO_2 (Akhlaq, 1999). As a result, the potential of crude oils could be linked to their polar signature, indicating their favourable reactions to micro-dispersion formation, and the peak areas corresponding to bond abundance can be identified.

As for Crude A, its intensity of the C=O, C=C, and O–H bonds is found to increase significantly when HSW is switched to LSW and then to LSW + CO_2 (Fig. 8 and Table 5). Such an increased intensity can be attributed to both a large concentration of surface-active substances made up of the C=O and C=C bonds and an increase in water molecules close to the interface (Mehraban et al., 2022). Then, it can be inferred that polar acidic substances facilitate forming micro-dispersions and that the presence of CO_2 accelerates such an in-situ formation. All Crude A samples indicate that the primary interactions occurring on the other side of the interface is

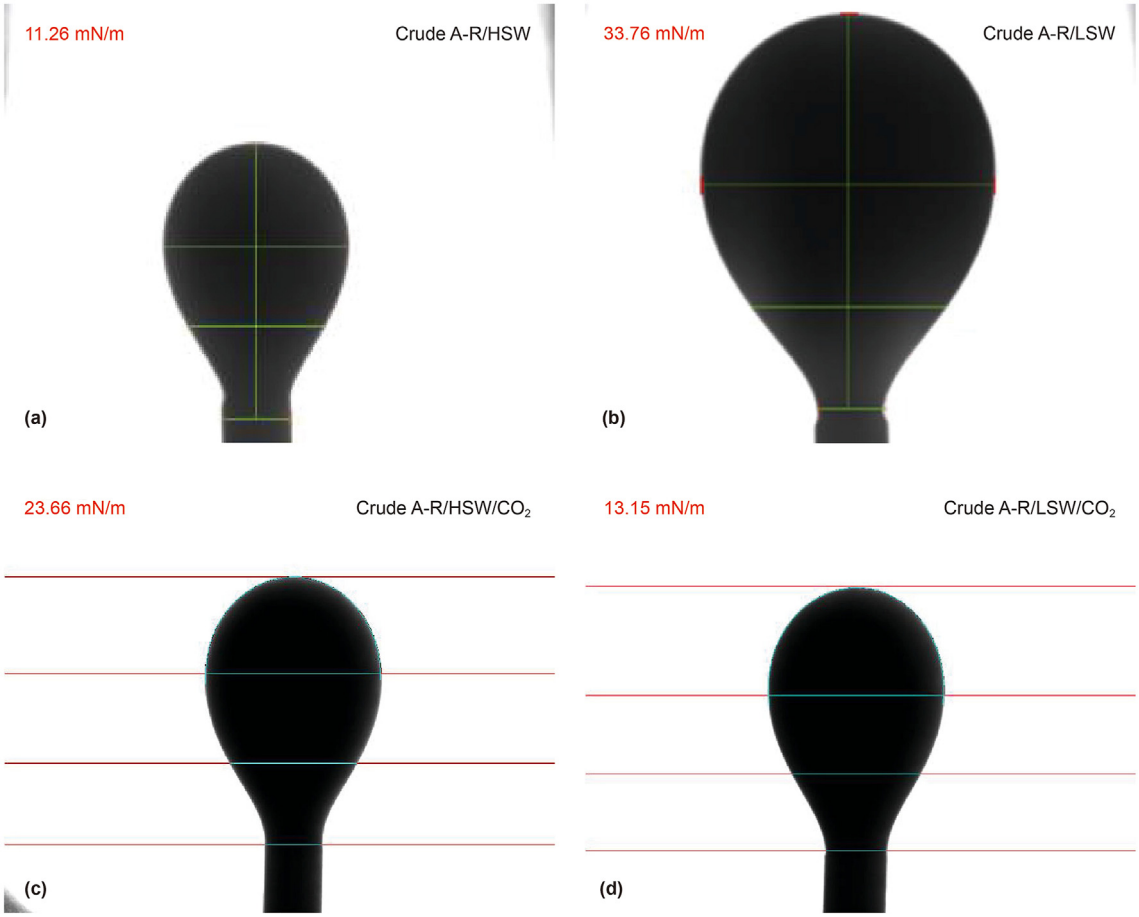

Fig. 12. Measured IFT for different systems at 60 °C and 10 MPa. **(a)** Crude A-R/HSW; **(b)** Crude A-R/LSW; **(c)** Crude A-R/HSW/CO_2; **(d)** Crude A-R/LSW/CO_2.

the micro-dispersion induced by acidic chemicals. As for Crude A-R, its intensity of the C=O, C=C, and O–H bonds is found to increase when HSW is switched to LSW and then to LSW + CO_2, although the difference is not noticeable (Fig. 9 and Table 5). It can be concluded that the extent of micro-dispersion formation is not substantial in Crude A-R and our previous experimental procedure for the separation of micro-dispersion is effective.

3.3. Surface charges

Through easing the prerequisites for other suggested mechanisms including pH-induced wettability alteration (Austad et al., 2010; Aksulu et al., 2012) and MIE (Mehraban et al., 2021), EDL has been suggested as a driving force for an initiative to impose a major impact on oil recovery.

As kaolinite and montmorillonite are the common components of the sandstone core, their surface charges of these two well-known clay minerals along with those of Crude A and Crude A-R samples were measured and presented in Fig. 10. In LSW, the surface charges of kaolinite particles and Crude A are measured to be −22.54 and −45.92 mV, respectively. At a lower salinity, not only will the surface charges of mineral particles be negative, but also a stronger negative reaction is initiated from the surface charges of Crude A and Crude A-R, indicating a greater adsorption of negatively charged surface-active components onto the interface.

The intense screening effect (i.e., shielding effect) occurring at the interface (Fathi et al., 2012), which prevents the adsorption of surface-active components onto the interface from the bulk oil, might be a consequence of the surface charges of crude oil samples approaching the point of zero charges at a higher salinity (Mahani et al., 2015a; Chavez-Miyauchi et al., 2016). The EDL theory states that these negative surface charges would result in a significant electrostatic repulsion between the oil/brine and rock/brine interfaces, altering the wettability toward a more water-wet condition (Ligthelm et al., 2009; Lee et al., 2010; Mahani et al., 2015b). According to these observations from both tests utilizing Crude A and Crude A-R, injection of LSW should trigger the EDL expansion.

3.4. IFT measurements

Significant distinctions in microscopic displacement efficiency of a CO_2-LSWAG process may originate from chemical interactions among gas, brine, and crude oil. When it comes to two-phase flow, the IFTs of the Crude A/HSW (Fig. 11(a)) and Crude A-R/HSW (Fig. 12(a)) are measured to be 6.46 and 11.26 mN/m, respectively, and the measured IFTs of the Crude A/LSW (Fig. 11(b)) and Crude A-R/LSW (Fig. 12(b)) are 21.79 and 33.76 mN/m, respectively. Both Crude A (which has a significant tendency to form micro-dispersions) and Crude A-R (without micro-dispersion) exhibit an increase in oil/brine IFT with a decrease in salinity. Consequently, it is determined that such a decreased in IFT (as in the situation of surfactant) fails to be the mechanism through which more significant oil recovery may be acquired in a LSWI process as noted by Alameri et al. (2014). Even so, we can observe that the IFTs between Crude A and brine were always lower than those between Crude A-R and brine. This can be attributed to the smaller the polarity

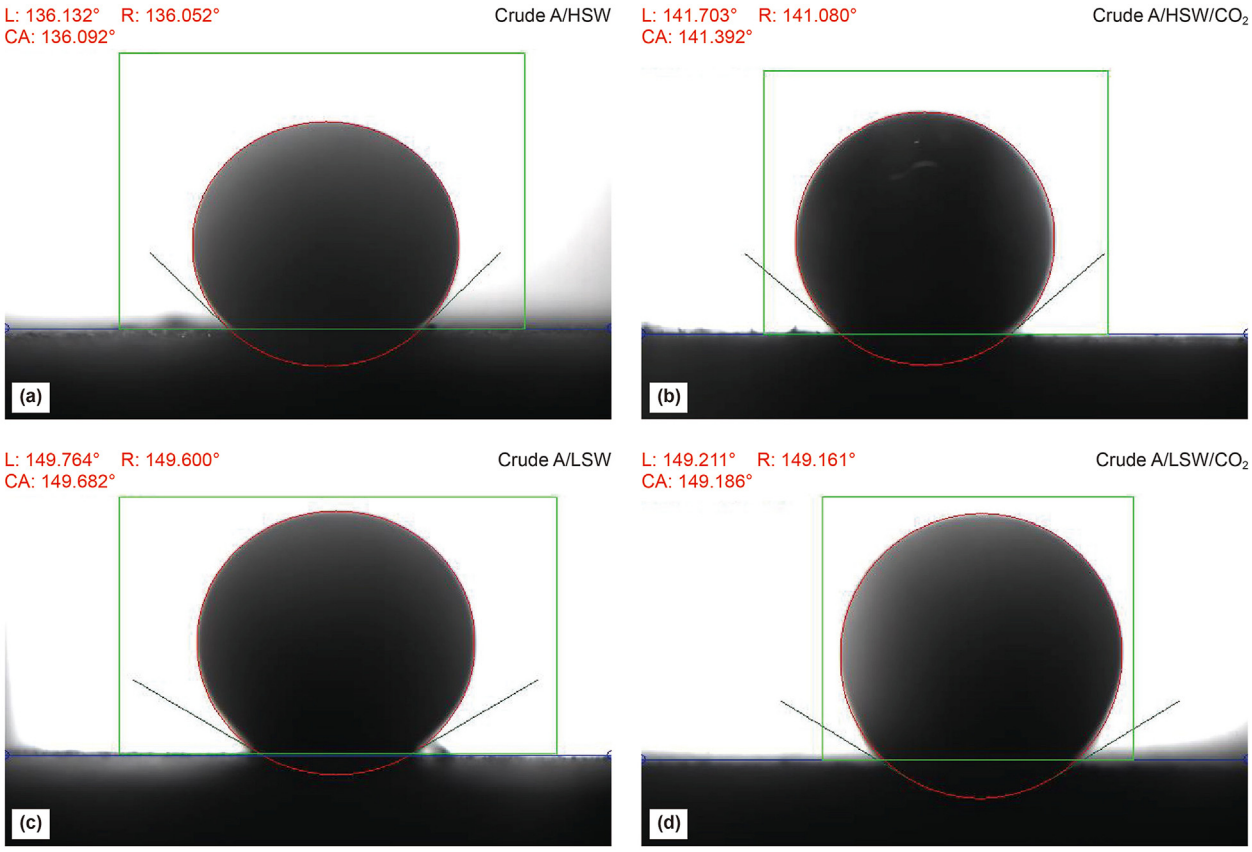

Fig. 13. Contact angle of cleaned un-aged sandstone thin slices at 60 °C and 10 MPa. (**a**) Thin slice #1-1/Crude A/HSW system; (**b**) Thin slice #1-1/Crude A/HSW/CO_2 system; (**c**) Thin slice #1-2/Crude A/LSW system; (**d**) Thin slice #1-2/Crude A/LSW/CO_2 system.

difference of the two phase molecules (i.e., the smaller the free surface energy). Nevertheless, a reduction in brine salinity might be beneficial for the oil/brine IFT in the scenario of combining LSWI and CO_2 as an alternating scheme or a continuous one.

To investigate this hypothesis, after evaluating the oil/brine IFTs (two-phase flow), CO_2 was introduced to form a three-phase flow system so as to examine how it affects IFTs. Results indicated that the IFTs were lower in the three-phase system than the two-phase systems. The IFTs of the Crude A/HSW/CO_2 (Fig. 11(c)) and Crude A-R/HSW/CO_2 (Fig. 12(c)) are found to be 10.92 and 23.66 mN/m, respectively, and the IFTs of the Crude A/LSW/CO_2 (Fig. 11(d)) and Crude A-R/LSW/CO_2 (Fig. 12(d)) are 5.84 and 13.15 mN/m, respectively. A decrease in the IFTs of three-phase oil/brine/CO_2 system could arise from an increase in CO_2 solubility with low-salinity brine. Compared to Crude A-R/brine/CO_2, the IFTs of Crude A/brine/CO_2 revealed a similar pattern but lower than those of the Crude A-R/brine/CO_2 systems. This might be ascribed to the fact that more CO_2 was dissolved into Crude A (which has an intense propensity to form micro-dispersion) than brine so as to reduce the density difference between the oil and brine. Nevertheless, if CO_2 is injected below its MMP, brine/oil IFT reduction through CO_2 dissolution in oil is less probable. According to multiple studies utilizing the molecular dynamics simulation, the IFT differential between oil/brine and CO_2/brine is responsible for driving CO_2 accumulation and diffusion at the oil/water interface (Liu et al., 2016; Mohammed and Mansoori, 2018). It is noteworthy to mention that the IFT (5.84 mN/m) for Crude A/LSW/CO_2 was lower than that (6.46 mN/m) for Crude A/HSW. This finding is consistent with the measured water content of crude oil by using the FTIR analysis. As a result, imbibition and oil mobilization may be affected by the IFT reduction and the corresponding reduction of capillary pressure due to CO_2 dissolution, reducing residual oil saturation and thus increasing oil recovery.

3.5. Wettability measurements

Due to the density of oil being lower than that of brine, the contact angles of oil/brine and oil/brine/CO_2 systems in the respective presence of aged and un-aged sandstone core samples were measured by forming a sessile oil drop below the rock slice. Both the left and right angles at the three-phase points were measured and then an arithmetic average was obtained. Reservoir rocks are categorized as water-wet, medium-wet, or oil-wet when the angles at which water adheres to a rock surface are 0°–75°, 75°–105°, and 105°–180°, respectively (Anderson, 1986). Contact angle measurements of cleaned un-aged thin slices are shown in Figs. 13 and 14, while those of crude-aged thin slices are shown in Figs. 15 and 16.

As for the Crude A/brine systems of cleaned un-aged thin slices, the contact angle is decreased from around 44° in HSW (Fig. 13(a)) to approximately 31° in LSW (Fig. 13(c)); Similarly, the contact angle is decreased from around 47° in HSW (Fig. 14(a)) to approximately 36° in LSW (Fig. 14(c)) for the Crude A-R/brine system of cleaned un-aged thin slices. Moreover, the diffusion of CO_2 has almost no effect on the wettability of un-aged thin slices in all the oil/brine systems (Fig. 13(b) and (d), Fig. 14(b) and (d)). This is a negative environment for achieving wettability alterations, which is required to develop the CO_2-LSWAG advantage (Dang et al., 2016).

As for Crude A, the measured contact angles indicate how the in-

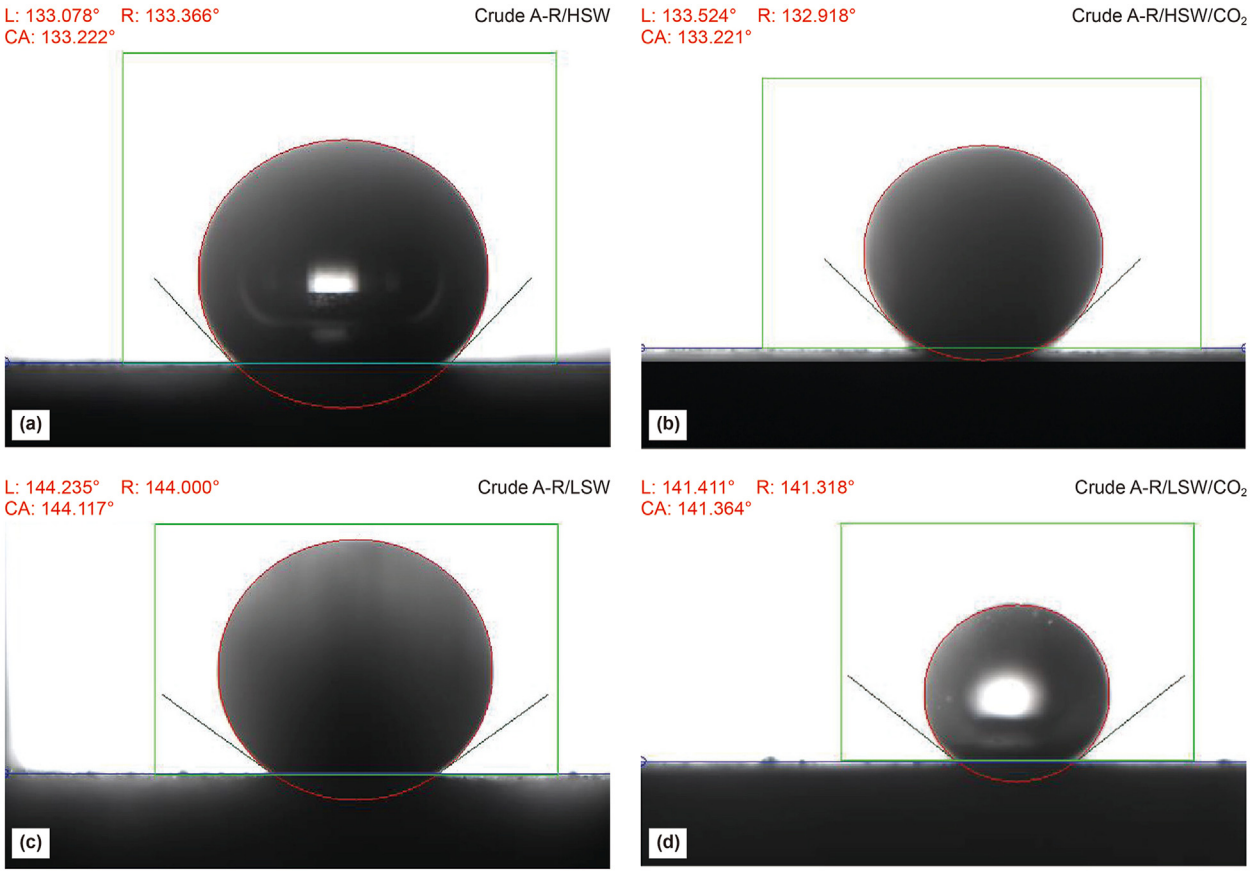

Fig. 14. Contact angle of cleaned and un-aged sandstone thin slices at 60 °C and 10 MPa. **(a)** Thin slice #1-3/Crude A-R/HSW system; **(b)** Thin slice #1-3/Crude A-R/HSW/CO_2 system; **(c)** Thin slice #1-4/Crude A-R/LSW system; **(d)** Thin slice #1-4/Crude A-R/LSW/CO_2 system.

situ formed micro-dispersion significantly alters wettability in oil-wet porous media (Figs. 15 and 16). For Crude A (Fig. 15(a) and (c)), the contact angle measured in LSW is 44° lower than that in HSW (approximately 144°), and this wettability alteration facilitates increasing oil recovery from a LSWI process (Mehraban et al., 2022). Such wettability alteration results from the in-situ formed micro-dispersion as observed from mixed-wet micromodels (Emadi and Sohrabi, 2013; Mahzari et al., 2018). As for Crude A-R, nevertheless, an unnoticeable difference in the measured contact angles between HSW and LSW can be observed (Fig. 16(a) and (c)). Apparently, thin slice #1-3 aged with Crude A-R (Fig. 16(a)) is found to be slightly more hydrophilic compared with thin slice #1-1 aged with Crude A (Fig. 15(a)). This can be ascribed to the fact that removing the surface-active components of the oil reduces its ability to initiate a mixed-wet or an oil-wet wettability in a rock (Sohrabi et al., 2017). Despite Crude A-R and clay particles exhibit intense electrostatic repulsion between oil/brine and rock/brine interfaces, as described in Section 3.3, the EDL principle cannot be applied herein as there was no wettability alteration.

Due to the dissolution of CO_2 in LSW, wettability of the reservoir rock may be altered toward a mixed-wet or water-wet condition so that oil recovery is increased (Yang et al., 2008a, 2008b; Teklu et al., 2016). For thin slices aged with oil, it is significant to note that the contact angles measured in the Crude A/LSW/CO_2 system (Fig. 15(d)) and Crude A-R/LSW/CO_2 system (Fig. 16(d)) are 53° and 109°, respectively. As such, the strong propensity of Crude A with respect to micro-dispersion formation is responsible for the wettability alteration of the former. In other words, the dissolution of CO_2 in crude oil and CO_2 concentration and diffusion at the oil/water interface should contribute positively to wettability alteration.

3.6. NMR monitored-displacement tests

Despite the fact that sandstone cores were utilized in this work to characterize micro-dispersion, previous research has revealed how crucial the micro-dispersion is evolved in a carbonate reservoir (Al-Hammadi et al., 2018). As a consequence, appropriate results from this research could also be applied to carbonate reservoirs. After discovering that the EDL expansion for Crude A and Crude A-R in the planned coreflood samples with sandstone rich in clay minerals is almost the same, the MIE mechanism shall be partially responsible for the increased oil recovery due to the presence of Ca^{2+} in the formation water and clay in the core composition. As a result, removing the natural reverse micelles of Crude A before the tests is to blame for the only variable in the oil recovery results.

The oil recovery factors of Samples #1 and #3 as opposed to the injected PV of various fluids are depicted in Fig. 17(a) and (c). During secondary waterflooding with 10 PVs of HSW, 42.34% of the original oil in place (OOIP) was recovered in Sample #1 and 42.72% of the OOIP was recovered in Sample #3, respectively. As the tertiary recovery scenario, one cycle of immiscible CO_2-HSWAG process with 5 PVs of water and 3 PVs of CO_2 was performed in Sample #1 with an incremental oil recovery of 12.35% and in Sample #3 with an incremental oil recovery of 12.53%, respectively. The

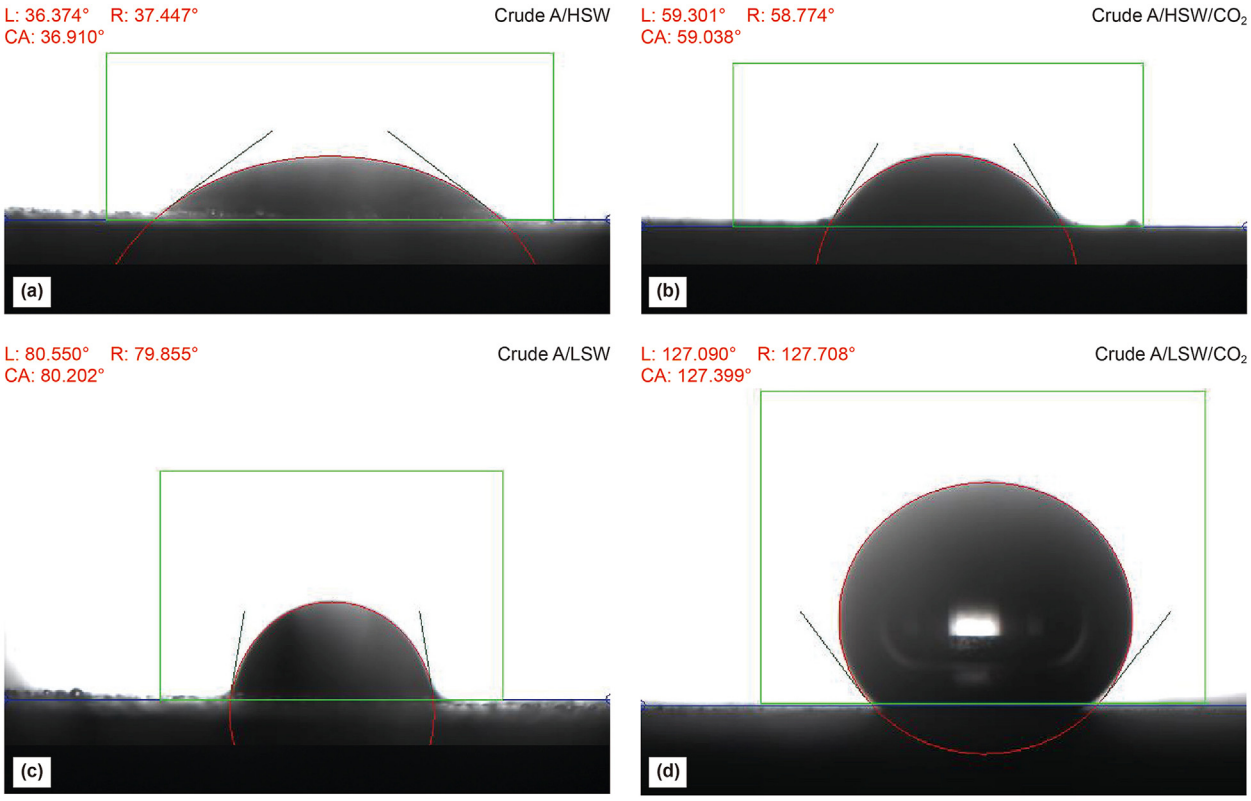

Fig. 15. Contact angle of Crude A-aged sandstone thin slices at 60 °C and 10 MPa. **(a)** Thin slice #1-1/Crude A/HSW system; **(b)** Thin slice #1-1/Crude A/HSW/CO_2 system; **(c)** Thin slice #1-2/Crude A/LSW system; **(d)** Thin slice #1-2/Crude A/LSW/CO_2 system.

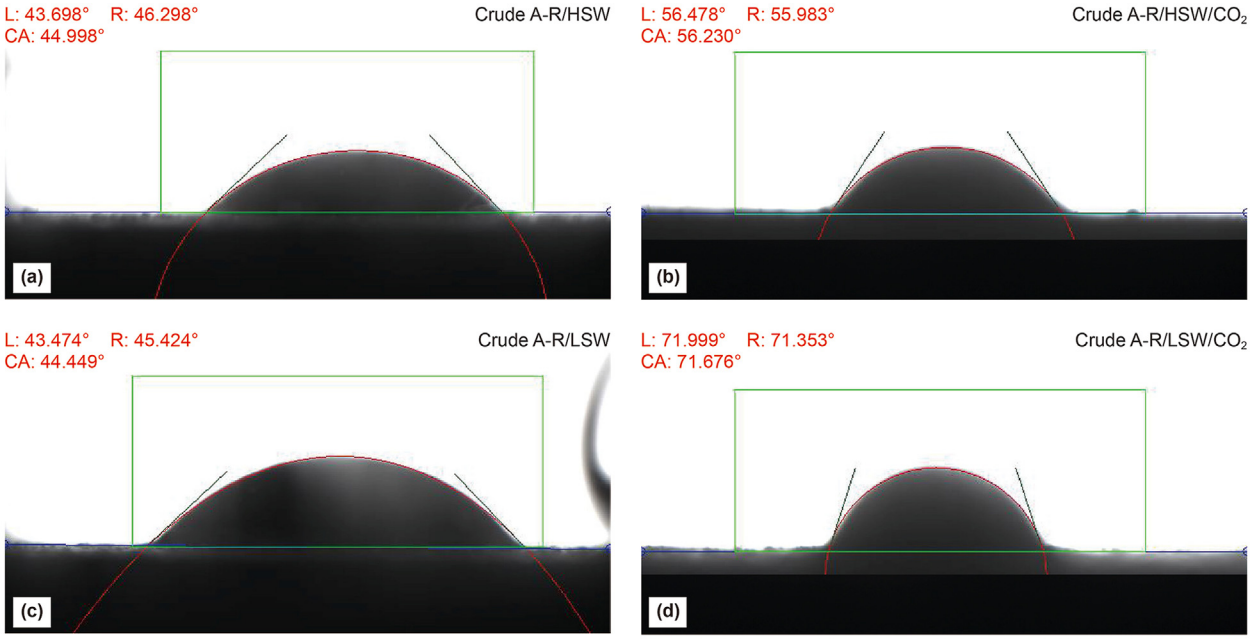

Fig. 16. Contact angle of Crude A-R-aged sandstone thin slices at 60 °C and 10 MPa. **(a)** Thin slice #1-3/Crude A-R/HSW system; **(b)** Thin slice #1-3/Crude A-R/HSW/CO_2 system; **(c)** Thin slice #1-4/Crude A-R/LSW system; **(d)** Thin slice #1-4/Crude A-R/LSW/CO_2 system.

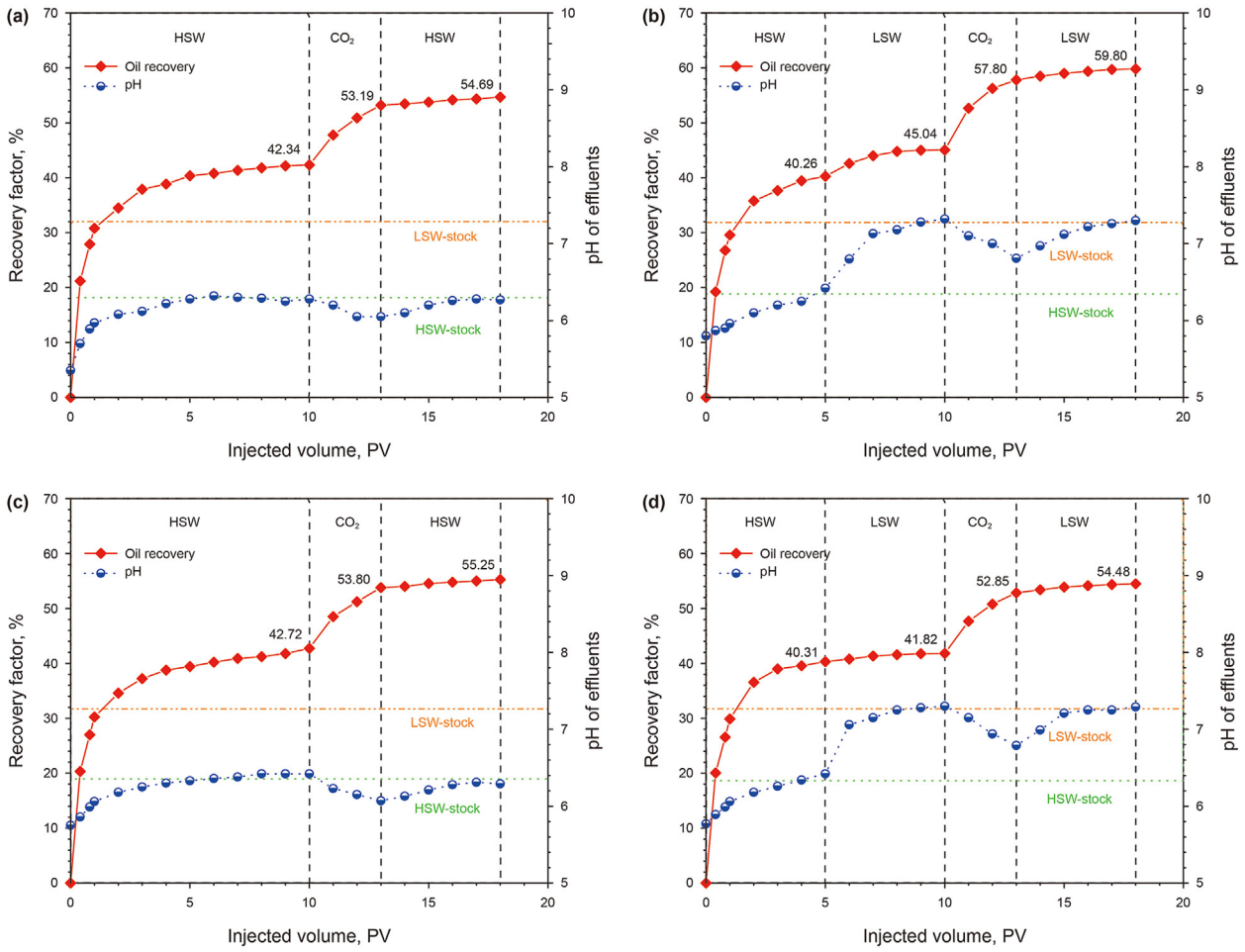

Fig. 17. Oil recovery and pH of the coreflooding experiments. **(a)** Sample #1 saturated with Crude A; **(b)** Sample #2 saturated with Crude A; **(c)** Sample #3 saturated with Crude A-R; **(d)** Sample #4 saturated with Crude A-R.

injected CO_2 leads to an increase in oil recovery, though the salinity of the injected brine remains unchanged in Samples #1 and #3. Considering the fact that CO_2 was injected at immiscible condition which hindered gas dissolution in the oil phase to a certain degree, the dissolved CO_2 in the injected brine with a high salinity regulates CO_2 override and thus increases the CO_2 distribution range.

Similar procedures were carried out in Samples #2 and #4, with the exception that the injected brine employed in the tertiary recovery stage was LSW (Fig. 17(b) and (d)). During the secondary waterflooding stage, 5 PVs of HSW recovered 40.26% of OOIP in Sample #2 and 40.31% of OOIP in Sample #4, respectively. It is essential to note that, after switching the injection fluid to LSW for 5 PVs in the tertiary recovery stage, the incremental oil recovery factors in Samples #2 and #4 were found to be 4.78% and 1.51% of OOIP, respectively. Before additional oil could be produced, 1 PV of LSW was needed, which is similar with the previous study (Mehraban et al., 2022). This revealed that the incremental oil recovery results from the formation of micro-dispersion and this process is relatively time-consuming. Subsequently, one cycle of CO_2-LSWAG was injected, yielding an incremental oil recovery of 14.76% and 12.66% of OOIP in Samples #2 and #4, respectively. This can be attributed to Sample #2 saturated with Crude A having more CO_2 to diffuse into the oil phase and reach the oil-water interface, hence facilitating wettability alteration to a water-wet environment (Moradpour et al., 2021). Regarding Crude A-R, a comparison of the residual oil saturation and recovery factor in Samples #3 and #4 reveals that the CO_2-LSWAG process was not more successful than the CO_2-HSWAG process. In this way, during the LSWI process, the increased oil recovery was not aided by the presence of clay minerals. Additionally, the higher recovery factor via the former is not triggered by the increased CO_2 solubility in LSW (Teklu et al., 2016). As such, it can be stated that the additional oil recovery for Samples #2 and #4 during the tertiary CO_2-LSWAG is directly proportional to the amount of the in-situ formed micro-dispersions.

The pore size distribution of the four core plugs was determined by using the NMR analysis after we thoroughly saturated them with high-salinity brines (Fig. 18). It is clear that the pore size distributions of Samples #1–#4 are comparable. Considering D_2O in pores before being saturated with oil lacks hydrogen atoms, the T_2 spectrum from the saturated oil to irreducible water in the NMR tests indicated both the oil distribution and cumulative pore volume in a core plug (Wang et al., 2023). Fig. 18(b) shows that, during the tertiary LSWI, the T_2 spectrum of Sample #2 lost the oil signal between 80 and 115 ms, implying that the displacement of huge clusters of remaining oil in large pores. This is a phenomenon not observed in other core plugs, indicating that Sample #2 is altered from oil-wet to water-wet as a result of the in-situ formation of micro-dispersion with capillary force having a greater impact than the viscous force. During the tertiary LSWI, the trapped oil is more easily retrieved since water must flow to a larger pore and its flowing to a narrower pore was prevented by the in-situ formed

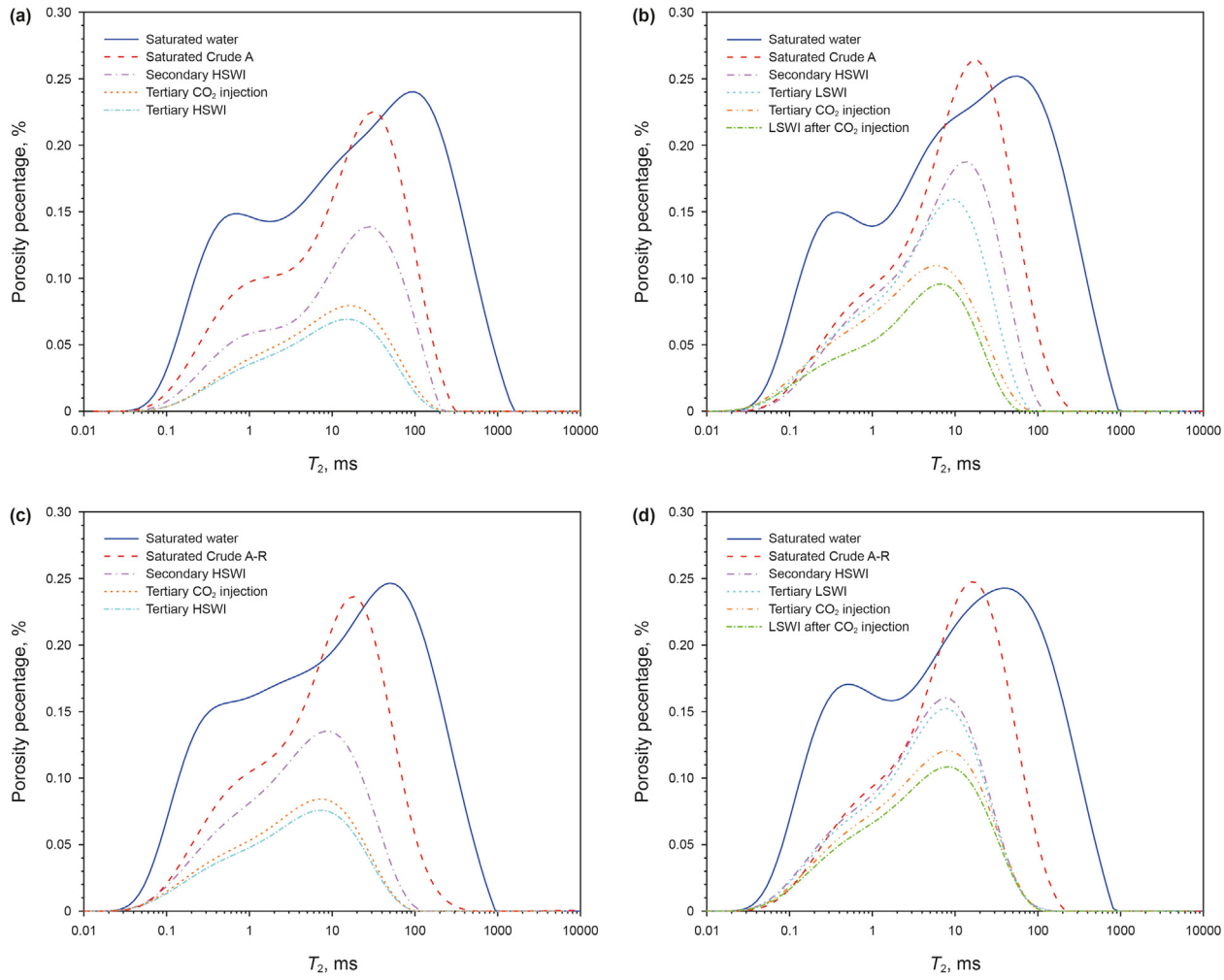

Fig. 18. NMR T_2 spectra of Samples #1 (**a**), #2 (**b**), #3 (**c**), and #4 (**d**).

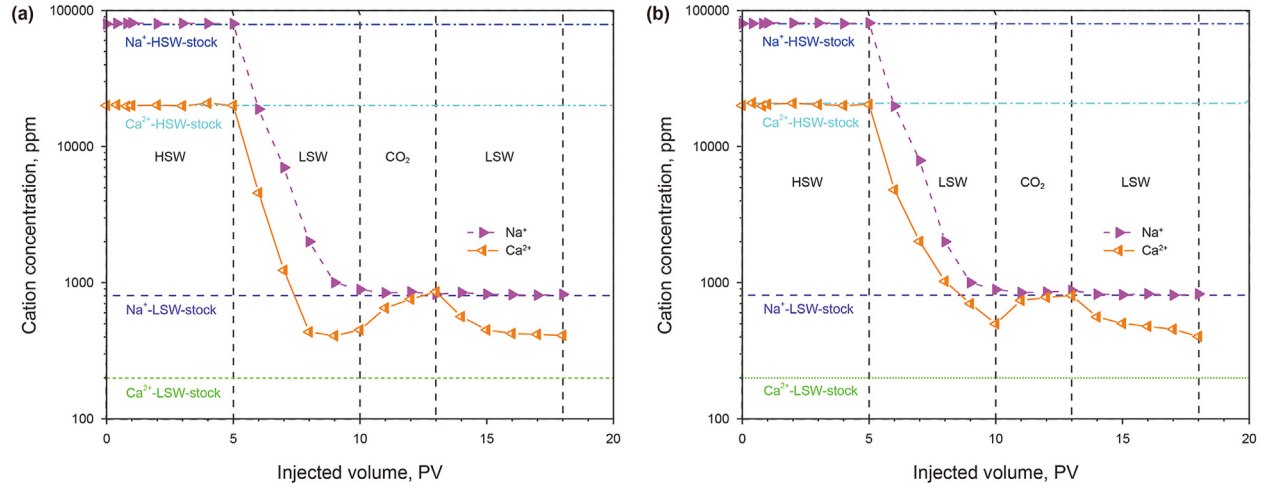

Fig. 19. Ionic concentration in the effluents in Samples #2 (**a**) and #4 (**b**).

micro-dispersions. This finding is similar to that visualized from a micro-model (Morishita et al., 2020).

In order to further clarify the CO_2-LSWAG mechanism, it is crucial to investigate the interactions among CO_2, the ions in the injection brines, and the rock surface. In this way, the aqueous effluents were analyzed using pH measurements and ion chromatography (IC). Compared to LSW, HSW is found to have a lower pH since it has a higher concentration of Ca^{2+} ions, leading to the

formation of $Ca(OH)_2$ with the consumption of hydroxide ions (OH^-) (Fig. 17(a) and (c)). During the LSWI periods, the pH is increased, indicating that there exist ionic interactions among aqueous solutions with high and low salinities within the core plugs (Fig. 17(b) and (d)). The dissolution of CO_2 into brine alters its pH, depending on brine salinity, rock type, and pressure (Almeida da Costa et al., 2021). As shown in Fig. 17, the pH is decreased with an increase in the injected volume; nevertheless, such a decrease is more aggressively with the LSW/CO_2 system. Although the pH of the core plugs is changed when CO_2 and other brines were put into them, the pH fluctuations in these studies do not show any association with the increased oil recovery.

Fig. 19 indicates the concentrations of Na^+ and Ca^{2+} ions in the effluents for Samples #2 and #4. In both tests, the Na^+ concentration reduces quickly after shifting to LSWI and returning to the LSW-stock value (i.e., the original concentration within LSW) within about 5 PVs. In contrast, although the concentration of Ca^{2+} began to fall immediately after switching to LSWI and has yet to achieve its stock value after 5 PVs, illustrating cation exchange occurs between the rock surface and the injection fluid. During all CO_2 injections, the Ca^{2+} effluent concentrations are increased, indicating that its absolute permeability is increased due to rock dissolution. Excessive CO_2 will impose a significant impact on this equilibrium, and calcite will dissolve if the acidity is too high (Note: The cores employed in this research included 2.03% calcite ($CaCO_3$)). Compared to Sample #2, Sample #4 exhibits a more severe Ca^{2+} cation exchange, although there exists a minor increase in oil recovery. The only variations that contributed to the increased oil recovery of Crude A during the CO_2-LSWAG process were the in-situ formed micro-dispersions, which leads to changes in IFT, wettability, CO_2 dissolution and diffusion.

4. Conclusions

In this work, well-designed and integrated experiments have been performed for the first time to characterize the in-situ formation of micro-dispersion and identify its EOR roles during a CO_2-LSWAG process under various conditions. The major findings are summarized as follows.

(1) The micro-dispersion ratio is increased monotonically as brine salinity is decreased, and the micro-dispersion of the oil/LSW/CO_2 is increased by 82.60% compared to that of the oil/LSW, indicating that CO_2 can facilitate the formation of micro-dispersion in the presence of LSW.
(2) Utilizing IR spectroscopy to perform a systematic investigation on the oil/brine and oil/brine/CO_2 interface compositions, it was demonstrated that, based on the salinity of the brine and the quantity of CO_2 injected, the chemical compositions of crude oil in contact with brine might vary dramatically. For CO_2-LSW mixtures, the polar and acidic molecules that make up the crude oil phase are essential.
(3) With a higher solubility in LSW and more molecular diffusion in the potent oil phase related to micro-dispersion, CO_2 promotes the oil mobilization by reducing the density difference between oil and water and altering the rock wettability towards more water-wet. The formation of micro-dispersion and the partitioning of surface-active materials are inversely related to the IFT and contact angle variations among crude oil/LSW/CO_2.
(4) Four NMR monitored-displacement analyses with a potent and a weak crude oil related to micro-dispersion in clay-rich sandstone cores revealed that fluid–fluid interactions controlled the incremental oil recovery with the CO_2-LSWAG process. Although a similar capability for cation exchange between the rock surface and the injection fluid and an identical volume of clay in experiments, the CO_2-LSWAG process was only found to result in a higher oil recovery with oil that has a significant potential of forming micro-dispersions.

Conflict of interest statement

The authors affirm that they have no known financial or interpersonal conflicts that would have appeared to have an impact on the research presented in this study.

Data availability

All the data are embedded in the paper.

CRediT authorship contribution statement

Jia-Xin Wang: Writing – original draft, Visualization, Methodology, Investigation, Formal analysis, Data curation. **Leng Tian:** Resources, Project administration, Funding acquisition, Conceptualization. **Can Huang:** Methodology, Investigation. **Xiao-Jiao Deng:** Supervision, Conceptualization. **Daoyong Tony Yang:** Writing – review & editing, Supervision, Methodology, Funding acquisition, Formal analysis, Conceptualization. **Rui-Heng Wang:** Methodology. **Jia-Hao Lin:** Conceptualization. **Jin-Yang Wei:** Investigation.

Acknowledgements

This work is support by The CO_2 Flooding and Storage Safety Monitoring Technology (Grant 2023YFB4104200), The Dynamic Evolution of Marine CO_2 Geological Sequestration Bodies and The Mechanism of Sequestration Efficiency Enhancement (Grant U23B2090), and The Efficient Development Technology and Demonstration Project of Offshore CO_2 Flooding (Grant KJGG-2022-12-CCUS-0203). The authors also appreciate The Natural Sciences and Engineering Research Council of Canada (NSERC) awarded D. Yang a Discovery Grant and a Collaborative Research and Development (CRD) Grant.

References

Afzal, S., Rezaei, N., Zendehboudi, S., 2018. A comprehensive review on enhanced oil recovery by water alternating gas (WAG) injection. Fuel 227, 218–246. https://doi.org/10.1016/j.fuel.2018.04.015.
Akhlaq, M.S., 1999. Characterization of the isolated wetting crude oil components with infrared spectroscopy. J. Pet. Sci. Eng. 22 (4), 229–235. https://doi.org/10.1016/S0920-4105(98)00079-5.
Aksulu, H., Hamso, D., Strand, S., et al., 2012. Evaluation of low-salinity enhanced oil recovery effects in sandstone: Effects of the temperature and pH gradient. Energy Fuels 26 (6), 3497–3503. https://doi.org/10.1021/ef300162n.
Al-Abri, H., Pourafshary, P., Mosavat, N., et al., 2019. A study of the performance of the LSWA CO_2 EOR technique on improvement of oil recovery in sandstones. Petroleum 5 (1), 58–66. https://doi.org/10.1016/j.petlm.2018.07.003.
Alameri, W., Teklu, T.W., Graves, R.M., et al., 2014. Wettability alteration during low-salinity waterflooding in carbonate reservoir cores. In: SPE Pacific Oil & Gas Conference and Exhibition. https://doi.org/10.2118/171529-MS.
Aleidan, A., Mamora, D., 2010. $SWACO_2$ and $WACO_2$ efficiency improvement in carbonate cores by lowering water salinity. In: SPE Canadian Unconventional Resources and International Petroleum Conference. https://doi.org/10.2118/137548-MS.
Al-Hammadi, M., Mahzari, P., Sohrabi, M., 2018. Fundamental investigation of underlying mechanisms behind improved oil recovery by low salinity-water injection in carbonate rocks. Fuel 220 (15), 345–357. https://doi.org/10.1016/j.fuel.2018.01.136.
Almeida da Costa, AA., Costa, G., Embirucu, J.B., et al., 2021. The influence of rock composition and pH on reservoir wettability for low-salinity water-CO_2 enhanced oil recovery applications in Brazilian Reservoirs. In: SPE Reserv Eval Eng 24 (1), 45–65. https://doi.org/10.2118/195982-PA.
Alotaibi, M.B., Nasr-El-Din, H.A., Fletcher, J.J., 2011. Electrokinetics of limestone and

dolomite rock particles. SPE Reserv Eval Eng 14 (5), 594–603. https://doi.org/10.2118/148701-PA.
Alotaibi, M.B., Yousef, A., 2016. The role of individual and combined ions in water flooding carbonate reservoirs: Electrokinetic study. SPE Res Eval Eng 20 (1), 77–86. https://doi.org/10.2118/177983-PA.
Anderson, W.G., 1986. Wettability literature survey-Part 1: Rock/oil/brine interactions and the effects of core handling on wettability. J Pet Technol 38 (10), 1125–1144. https://doi.org/10.2118/13932-PA.
Arhuoma, M., Yang, D., Dong, M., et al., 2009a. Numerical simulation of displacement mechanisms for enhancing heavy oil recovery during alkaline flooding. Energy Fuels 23 (12), 5995–6002. https://doi.org/10.1021/ef900690y.
Arhuoma, M., Dong, M., Yang, D., et al., 2009b. Determination of water-in-oil emulsion viscosity in porous media. Ind. Eng. Chem. Res. 48 (15), 7092–7102. https://doi.org/10.1021/ie801818n.
Austad, T., RezaeiDoust, A., Puntervold, T., 2010. Chemical mechanism of low-salinity water flooding in sandstone reservoirs. In: SPE Improved Oil Recovery Symposium. https://doi.org/10.2118/129767-MS.
Belazreg, L., Mahmood, S.M., 2020. Water alternating gas incremental recovery factor prediction and WAG pilot lessons learned. J. Pet. Explor. Prod. Technol. 10, 249–269. https://doi.org/10.1007/s13202-019-0694-x.
Bhadran, V., Goharzadeh, A., Yit Fatt, Y., 2019. Experimental study of oil recovery by water alternating gas (WAG) process in microporous media. J Phys Conf Ser 1276, 12–23. https://doi.org/10.1088/1742-6596/1276/1/012023.
Buckley, J., Takamura, K., Morrow, N., 1989. Influence of electrical surface charges on the wetting properties of crude oils. SPE Reserv Eng 4 (3), 332–340. https://doi.org/10.2118/16964-PA.
Buckley, J., Morrow, N., 1990. Characterization of crude oil-wetting behavior by adhesion tests. In: SPE/DOE Enhanced Oil Recovery Symposium. https://doi.org/10.2118/20263-MS.
Caudle, B.H., Dyes, A.B., 1958. Improving miscible displacement by gas-water injection. Trans. AIME 213, 281–283. https://doi.org/10.2118/911-G.
Chai, X., Tian, L., Dong, P., et al., 2022. Study on recovery factor and interlayer interference mechanism of multilayer co-production in tight gas reservoir with high heterogeneity and multi-pressure systems. J. Petrol. Sci. Eng. 210, 109699. https://doi.org/10.1016/j.petrol.2021.109699.
Chavez-Miyauchi, T.E., Firoozabadi, A., Fuller, G.G., 2016. Nonmonotonic elasticity of the crude oil-brine interface in relation to improved oil recovery. Langmuir 32 (9), 2192–2198. https://doi.org/10.1021/acs.langmuir.5b04354.
Cissokho, M., Bertin, H., Boussour, S., et al., 2010. Low-salinity oil recovery on clayey sandstone: Experimental study. Petrophysics 51 (5), 305–313.
Dang, C., Nghiem, L., Chen, Z., et al., 2014. CO_2 low-salinity water alternating gas: A new promising approach for enhanced oil recovery. In: SPE Improved Oil Recovery Symposium. https://doi.org/10.2118/169071-MS.
Dang, C., Nghiem, L., Nguyen, N., et al., 2016. Evaluation of CO_2 low-salinity water-alternating-gas for enhanced oil recovery. J. Nat. Gas Sci. Eng. 35, 237–258. https://doi.org/10.1016/j.jngse.2016.08.018.
Emadi, A., Sohrabi, M., 2013. Visual investigation of oil recovery by low-salinity water injection: Formation of water micro-dispersions and wettability alteration. In: SPE Annual Technical Conference and Exhibition. https://doi.org/10.2118/166435-MS.
Fathi, H., Kelly, J.P., Vasquez, V.R., et al., 2012. Ionic concentration effects on reverse micelle size and stability: Implications for the synthesis of nanoparticles. Langmuir 28 (25), 9267–9274. https://doi.org/10.1021/la300586f.
Ghasemian, J., Riahi, S., 2021. Effects of salinity and ionic composition of smart water on mineral scaling in carbonate reservoirs during water flooding. Pet Explor Dev 48 (2), 421–429. https://doi.org/10.1016/S1876-3804(21)60033-2.
Ghedan, S., 2009. Global laboratory experience of CO_2-EOR flooding. In: SPE/EAGE Reservoir Characterization and Simulation Conference. https://doi.org/10.2118/125581-MS.
Hadia, N., Hansan, T., Tweheyo, M., et al., 2012. Influence of crude oil components on recovery by high and low-salinity waterflooding. Energy Fuels 26 (7), 4328–4335. https://doi.org/10.1021/ef3003119.
Hilner, E., Andersson, M.P., Hassenkam, T., et al., 2015. The effect of ionic strength on oil adhesion in sandstone-the search for the low-salinity mechanism. Sci. Rep. 5 (1), 1–9. https://doi.org/10.1038/srep09933.
Huang, C., Tian, L., Wang, J., et al., 2024. Water-CO_2 wettability on sandstone surface with asphaltene adsorption: Molecular dynamics simulation. Fuel 360 (3), 130558. https://doi.org/10.1016/j.fuel.2023.130558.
Hunter, R.J., 1981. Potential in colloid science: Principles and applications. Academic Press, New York, USA.
Jaafar, M.Z., Vinogradov, J., Jackson, M.D., 2009. Measurement of streaming potential coupling coefficient in sandstones saturated with high-salinity NaCl brine. Geophys. Res. Lett. 36 (21), 1–6. https://doi.org/10.1029/2009GL040549.
Jadhunandan, P., 1990. Effects of brine composition, crude oil, and aging conditions on wettability and oil recovery. PhD Dissertation New Mexico Institute of Mining & Technology. Socorro, NM.
Jadhunandan, P., Morrow, N., 1991. Spontaneous imbibition of water by crude oil/brine/rock systems. In Situ, 15, pp. 90–109.
Jadhunandan, P., Morrow, N., 1995. Effect of wettability on waterflood recovery for crude-oil/brine/rock systems. SPE Reserv Eng 10 (1), 40–46. https://doi.org/10.2118/22597-PA.
Jiang, H., Nuryaningsih, L., Adidharma, H., 2010. The effect of salinity of injection brine on water alternating gas performance in tertiary miscible carbon dioxide flooding: Experimental study. In: SPE Western Regional Meeting. https://doi.org/10.2118/132369-MS.
Kulkarni, M.M., Rao, D.N., 2005. Experimental investigation of miscible and immiscible water-alternating-gas (WAG) process performance. J. Petrol. Sci. Eng. 48 (1–2), 1–20. https://doi.org/10.1016/j.petrol.2005.05.001.
Kumar, H.T., Shehata, A.M., Nasr-Ei-Din, H.A., 2016. Effectiveness of low-salinity and CO_2 flooding hybrid approaches in low-permeability sandstone reservoirs. In: SPE Trinidad and Tobago Section Energy Resources Conference. https://doi.org/10.2118/180875-MS.
Kunz, O., Klimeck, R., Wagner, W., et al., 2007. The GERG-2004 wide-range equation of state for natural gases and other mixtures. Verlag des Vereins Deutscher Ingenieure. Düsseldorf, Germany: European Gas Research Group (GERG) 322–323.
Lager, A., Webb, K.J., Black, C.J., 2007. Impact of brine chemistry on oil recovery. IOR 2007-14th European Symposium on Improved Oil Recovery. https://doi.org/10.3997/2214-4609-pdb.24.A24.
Lager, A., Webb, K.J., Black, C.J., et al., 2008. Low-salinity oil recovery-An experimental investigation. Petrophysics 49, 28–35.
Lee, S.Y., Webb, K.J., Collins, I., et al., 2010. Low-salinity oil recovery: Increasing understanding of the underlying mechanisms. In: SPE Improved Oil Recovery Symposium. https://doi.org/10.2118/129722-MS.
Ligthelm, D.J., Gronsveld, J., Hofman, J., et al., 2009. Novel waterflooding strategy by manipulation of injection brine composition. In: SPE EUROPEC/EAGE Conference and Exhibition. https://doi.org/10.2118/119835-MS.
Liu, B., Shi, J., Wang, M., et al., 2016. Reduction in interfacial tension of water-oil interface by supercritical CO_2 in enhanced oil recovery processes studied with molecular dynamics simulation. J. Supercrit. Fluids 111, 171–178. https://doi.org/10.1016/j.supflu.2015.11.001.
Mahani, H., Sorop, T., Ligthelm, D.J., et al., 2011. Analysis of field responses to low-salinity waterflooding in secondary and tertiary mode in Syria. In: SPE EUROPEC/EAGE Annual Conference and Exhibition. https://doi.org/10.2118/142960-MS.
Mahani, H., Keya, A.L., Berg, S., et al., 2015a. The effect of salinity, rock type and pH on the electrokinetics of carbonate-brine interface and surface complexation modeling. In: SPE Reservoir Characterisation and Simulation Conference and Exhibition. https://doi.org/10.2118/175568-MS.
Mahani, H., Keya, A.L., Berg, S., et al., 2015b. Insights into the mechanism of wettability alteration by low-salinity flooding (LSF) in carbonates. Energy Fuels 29 (3), 1352–1367. https://doi.org/10.1021/ef5023847.
Mahani, H., Menezes, R., Berg, S., et al., 2017. Insights into the impact of temperature on the wettability alteration by low-salinity in carbonate rocks. Energy Fuels 31 (8), 7839–7853. https://doi.org/10.1021/acs.energyfuels.7b00776.
Mahzari, P., Sohrabi, M., 2014. Crude oil/brine interactions and spontaneous formation of micro-dispersions in low-salinity water injection. In: The SPE Improved Oil Recovery Symposium. https://doi.org/10.2118/169081-MS.
Mahzari, P., Sohrabi, M., Cooke, A.J., et al., 2018. Direct pore-scale visualization of interactions between different crude oils and low-salinity brine. J. Petrol. Sci. Eng. 166, 73–84. https://doi.org/10.1016/j.petrol.2018.02.051.
McDonald, H., Bedwell, B., Gulari, E., 1986. FTIR spectroscopy of micro-emulsion structure. Langmuir 2, 704–708. https://doi.org/10.1021/la00072a005.
McGuire, P.L., Chatham, J.R., Paskvan, F.K., et al., 2005. Low-salinity oil recovery: An exciting new EOR opportunity for Alaska's North Slope. In: SPE Western Regional Meeting. https://doi.org/10.2118/93903-MS.
Mehraban, M.F., Farzaneh, S.A., Sohrabi, M., et al., 2020. Novel insights into the pore-scale mechanism of low-salinity water injection and the improvements on oil recovery. Energy Fuels 34 (10), 12050–12064. https://doi.org/10.1021/acs.energyfuels.0c01599.
Mehraban, M.F., Farzaneh, S.A., Sohrabi, M., 2021. Debunking the impact of salinity on crude oil/water interfacial tension. Energy Fuels 35 (5), 3766–3779. https://doi.org/10.1021/acs.energyfuels.0c03411.
Mehraban, M.F., Farzaneh, S.A., Sohrabi, M., et al., 2022. Fluid-fluid interactions inducing additional oil recovery during low-salinity water injection in inefficacious presence of clay minerals. Fuel 308, 121922. https://doi.org/10.1016/j.fuel.2021.121922.
Minch, R., 2018. Instruments and Methods for Optimization of Flooding Agents Used for Enhanced Oil Recovery. Krüss GmbH, Hamburg, Germany.
Mohammed, S., Mansoori, G.A., 2018. Molecular insights on the interfacial and transport properties of supercritical CO_2/brine/crude oil ternary system. J. Mol. Liq. 263, 268–273. https://doi.org/10.1016/j.molliq.2018.05.009.
Moradpour, N., Pourafshary, P., Zivar, D., et al., 2021. Experimental analysis of hybrid low-salinity water alternating gas injection and the underlying mechanisms in carbonates. J. Petrol. Sci. Eng. 202, 108562. https://doi.org/10.1016/j.petrol.2021.108562.
Morishita, R., Matsuyama, T., Ishiwata, Y., et al., 2020. Oil and water interactions during low-salinity enhanced oil recovery in water-wet porous media. Energy Fuels 34 (5), 5258–5266. https://doi.org/10.1021/acs.energyfuels.9b03753.
Nasralla, R.A., Bataweel, M.A., Nasr-El-Din, H.A., 2011. Investigation of wettability alteration by low-salinity water. In: SPE Offshore Europe. https://doi.org/10.2118/146322-MS.
Nasralla, R.A., Sergienko, E., Masalmeh, S.K., et al., 2014. Demonstrating the potential of low-salinity waterflood to improve oil recovery in carbonate reservoirs by qualitative coreflood. In: SPE Abu Dhabi International Petroleum Exhibition and Conference. https://doi.org/10.2118/172010-MS.
Pourafshary, P., Moradpour, N., 2016. Hybrid EOR methods utilizing low-salinity water. In: Samsuri, Ariffin (Ed.), Enhanced Oil Recovery Processes-New Technologies. IntechOpen, London, UK, pp. 1–25 (Chapter 1).
Qi, Z., Wang, Y., He, H., et al., 2013. Wettability alteration of the quartz surface in the

presence of metal. Energy Fuels 27, 7354–7359. https://doi.org/10.1021/ef401928c.
Ramanathan, R., Shehata, A.M., Nasr-El-Din, H.A., 2016. Effect of rock aging on oil recovery during water-alternating-CO_2 injection process: An interfacial tension, contact angle, coreflood, and CT scan study. In: SPE Improved Oil Recovery Conference. https://doi.org/10.2118/179674-MS.
RezaeiDoust, A., Puntervold, T., Austad, T., 2010. A discussion of the low-salinity EOR potential for a North Sea sandstone field. In: SPE Annual Technical Conference and Exhibition. https://doi.org/10.2118/134459-MS.
Rogers, J.D., Grigg, R.B., 2000. A literature analysis of the WAG injectivity abnormalities in the CO_2 process. SPE Reserv Eval Eng 4 (5), 375–386. https://doi.org/10.2118/73830-PA.
Rotondi, M., Callegaro, C., Masserano, F., et al., 2014. Low-salinity water injection: Eni's experience. In: SPE Abu Dhabi International Petroleum Exhibition and Conference. https://doi.org/10.2118/171794-MS.
Sandengen, K., Kristoffersen, A., Melhuus, K., et al., 2016. Osmosis as mechanism for low-salinity enhanced oil recovery. SPE J. 21 (4), 1227–1235. https://doi.org/10.2118/179741-PA.
Seccombe, J., Lager, A., Jerauld, G., et al., 2016. Demonstration of low-salinity EOR at interwell scale. Endicott Field, Alaska. In: SPE Improved Oil Recovery Symposium. https://doi.org/10.2118/129692-MS.
Shnoudeh, A.J., Hamad, I., Abdo, R.W., et al., 2019. Synthesis, characterization, and applications of metal nanoparticles. In: Tekade, R.K. (Ed.), Biomaterials and Bionanotechnology. Academic Press, Cambridge, pp. 527–612.
Siretanu, I., Ebeling, D., Andersson, M.P., et al., 2015. Direct observation of ionic structure at solid-liquid interfaces: A deep look into the Stern layer. Sci. Rep. 4 (1), 49–56. https://doi.org/10.1038/srep04956.
Skrettingland, K., Holt, T., Tweheyo, M., et al., 2011. Snorre low-salinity water injection-coreflooding experiments and single well field pilot. SPE Reserv Eval Eng 14 (2), 182–192. https://doi.org/10.2118/129877-PA.
Sohrabi, M., Mahzari, P., Farzaneh, J., et al., 2017. Novel insights into mechanisms of oil recovery by use of low-salinity-water injection. SPE J. 22, 407–416. https://doi.org/10.2118/172778-PA.
Tang, G.Q., Morrow, N.R., 1999. Influence of brine composition and fine migration on crude oil/brine/rock interactions and oil recovery. J. Petrol. Sci. Eng. 24 (2–4), 99–111. https://doi.org/10.1016/S0920-4105(99)00034-0.
Teklu, T.W., Alameri, W., Graves, R.M., et al., 2016. Low-salinity water-alternating-CO_2 EOR. J. Petrol. Sci. Eng. 142, 101–118. https://doi.org/10.1016/j.petrol.2016.01.031.
Wang, J., Tian, L., Wang, Z., et al., 2023. Performance evaluation of commingled production in a multilayer oil reservoir based on microscopic pore-throat structures. Fuel 348, 128482. https://doi.org/10.1016/j.fuel.2023.128482.
Wang, H., Tian, L., Gu, D., et al., 2020. Method for calculating non-Darcy flow permeability in tight oil reservoir. Transp Porous Media 133, 357–372. https://doi.org/10.1007/s11242-020-01427-8.
Wang, H., Tian, L., Chai, X., et al., 2022a. Effect of pore structure on recovery of CO_2 miscible flooding efficiency in low permeability reservoirs. J. Petrol. Sci. Eng. 208, 109305. https://doi.org/10.1016/j.petrol.2021.109305.
Wang, H., Tian, L., Huo, M., et al., 2022b. Dynamic track model of miscible CO_2 geological utilizations with complex microscopic pore-throat structures. Fuel 322, 124192. https://doi.org/10.1016/j.fuel.2022.124192.
Webb, K.J., Black, C.J., Al-Ajeel, H., 2004. Low-salinity oil recovery-log-inject-log. In: SPE/DOE Symposium on Improved Oil Recovery. https://doi.org/10.2118/89379-MS.
Wideroee, H.C., Rueslaatten, H., Boassen, T., et al., 2010. Investigation of low-salinity water flooding by NMR and CryoESEM. In: International Symposium of the Society of Core Analysts.
Yang, D., Gu, Y., 2005. Interfacial interactions between crude oil and CO_2 under reservoir conditions. Pet Sci Technol 23 (9), 1099–1112. https://doi.org/10.1081/LFT-200035536.
Yang, D., Gu, Y., Tontiwachwuthikul, P., 2008a. Wettability determination of the crude oil–reservoir brine–reservoir rock systems with dissolution of CO_2 at high pressures and elevated temperatures. Energy Fuels 22 (4), 2362–2371. https://doi.org/10.1021/ef800012w.
Yang, D., Gu, Y., Tontiwachwuthikul, P., 2008b. Wettability determination of the reservoir brine–reservoir rock systems with dissolution of CO_2 at high pressures and elevated temperatures. Energy Fuels 22 (1), 504–509. https://doi.org/10.1021/ef700383x.
Yang, D., Tontiwachwuthikul, P., Gu, Y., 2005. Interfacial tensions of the crude oil + reservoir brine + CO_2 systems at pressures up to 31 MPa and temperatures of 27°C and 58°C. J. Chem. Eng. Data 50 (4), 1242–1249. https://doi.org/10.1021/je0500227.
Yang, D., Song, C., Zhang, J., et al., 2015. Performance evaluation of injectivity for water-alternating-CO_2 processes in tight oil formations. Fuel 139, 292–300. https://doi.org/10.1016/j.fuel.2014.08.033.
Yousef, A.A., Al-Saleh, S., Al-Kaabi, A.U., et al., 2010. Laboratory investigation of novel oil recovery method for carbonate reservoirs. In: SPE Canadian Unconventional Resources and International Petroleum Conference. https://doi.org/10.2118/137634-MS.
Zhang, P., Tweheyo, M.T., Austad, T., 2006. Wettability alteration and improved oil recovery in chalk: The effect of calcium in the presence of sulfate. Energy Fuels 20 (5), 2056–2062. https://doi.org/10.1021/ef0600816.
Zolfaghari, H., Zebarjadi, A., Shahrokhi, O., et al., 2013. An experimental study of CO_2 low-salinity water alternating gas injection in sandstone heavy oil reservoirs. Iran J Oil Gas Sci Technol 2, 37–47. https://doi.org/10.22050/ijogst.2013.3643.